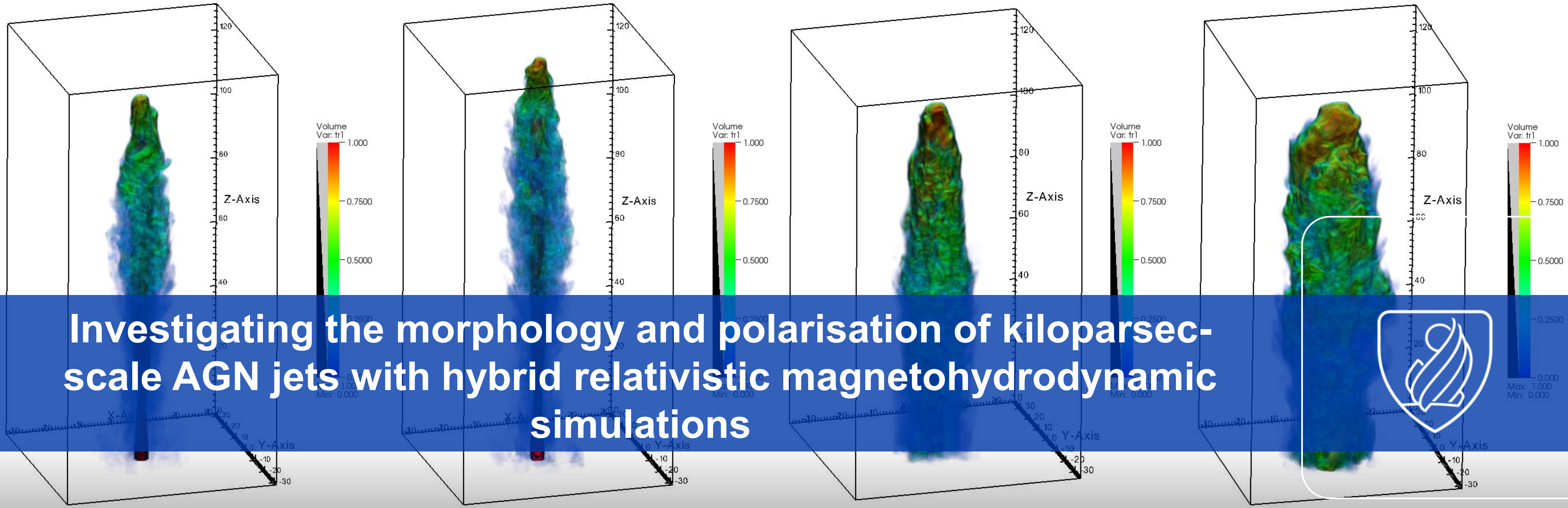

Investigating the morphology and polarisation of kiloparsec-scale AGN jets with hybrid relativistic magnetohydrodynamic simulations

www.ufs.ac.za

Izak van der Westhuizen, Reuben Immelman, Brian van Soelen and Bhargav Vaidya

Inspiring excellence, transforming lives through quality, impact, and care.

VISION 130
Renew and Reimagine for 2034

UNIVERSITY OF THE FREE STATE
UNIVERSITEIT VAN DIE VRYSTAAT
YUNIVESITHI YA FREISTATA

UFS NATURAL AND AGRICULTURAL SCIENCES

Active Galactic Nuclei

An active galactic nucleus (AGN) is the compact, highly luminous region at the center of a galaxy, powered by a supermassive black hole actively accreting gas and dust

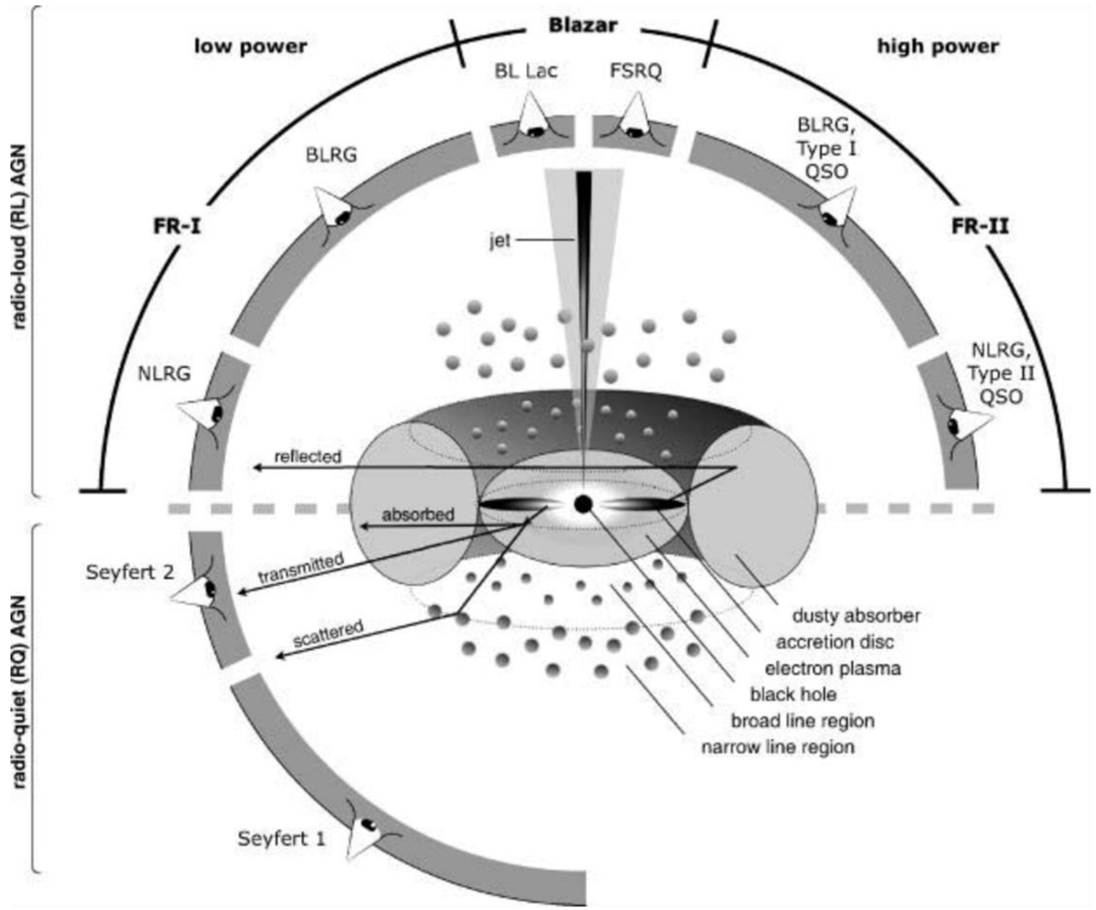

Beckmann and Shrader, 2012, Figure 4.16

Active Galactic Nuclei

Jetted (radio loud)

Radio galaxies

Radio loud Quasars

Blazars

Non-jetted (Radio

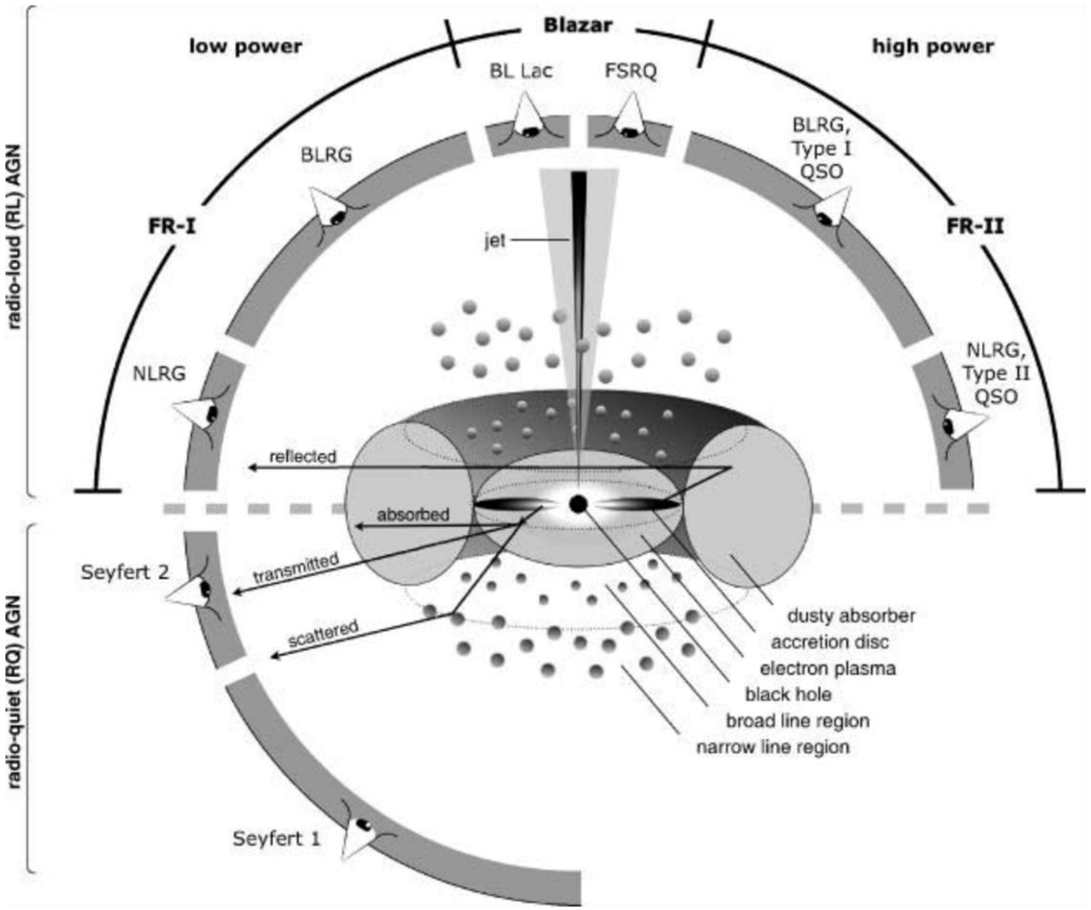

Beckmann and Shrader, 2012, Figure 4.16

Active Galactic Nuclei

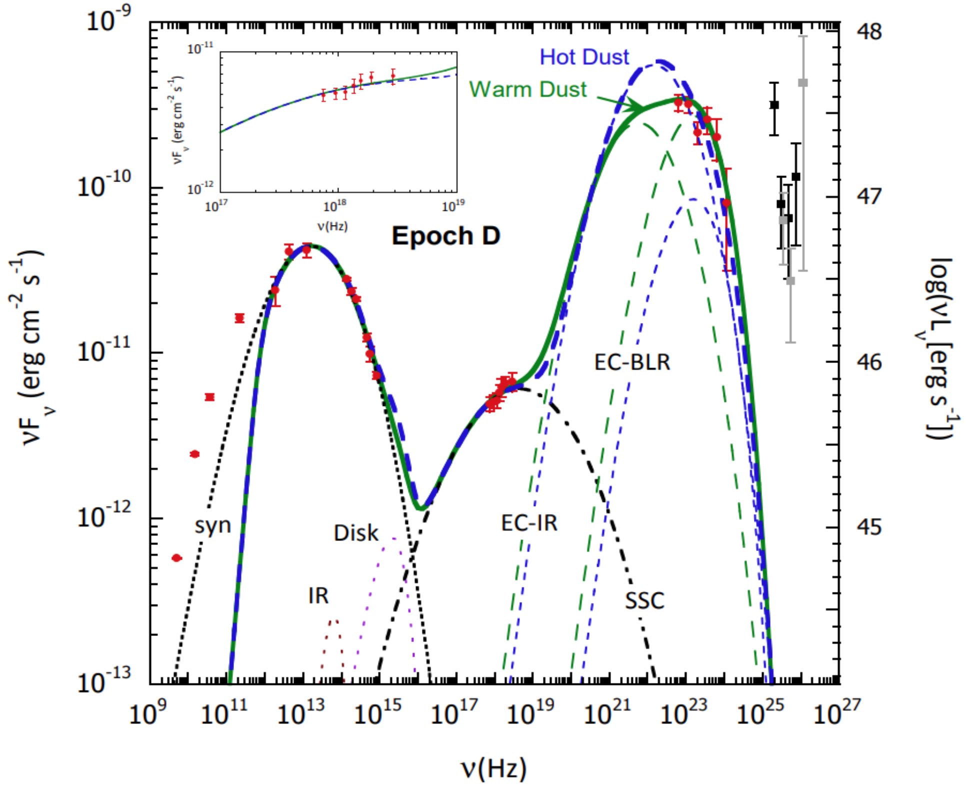

SED of 3C 279 with Leptonic emission models with contributions from different components in the AGN. Dermer, et al. 2014, ApJ, 782, 82

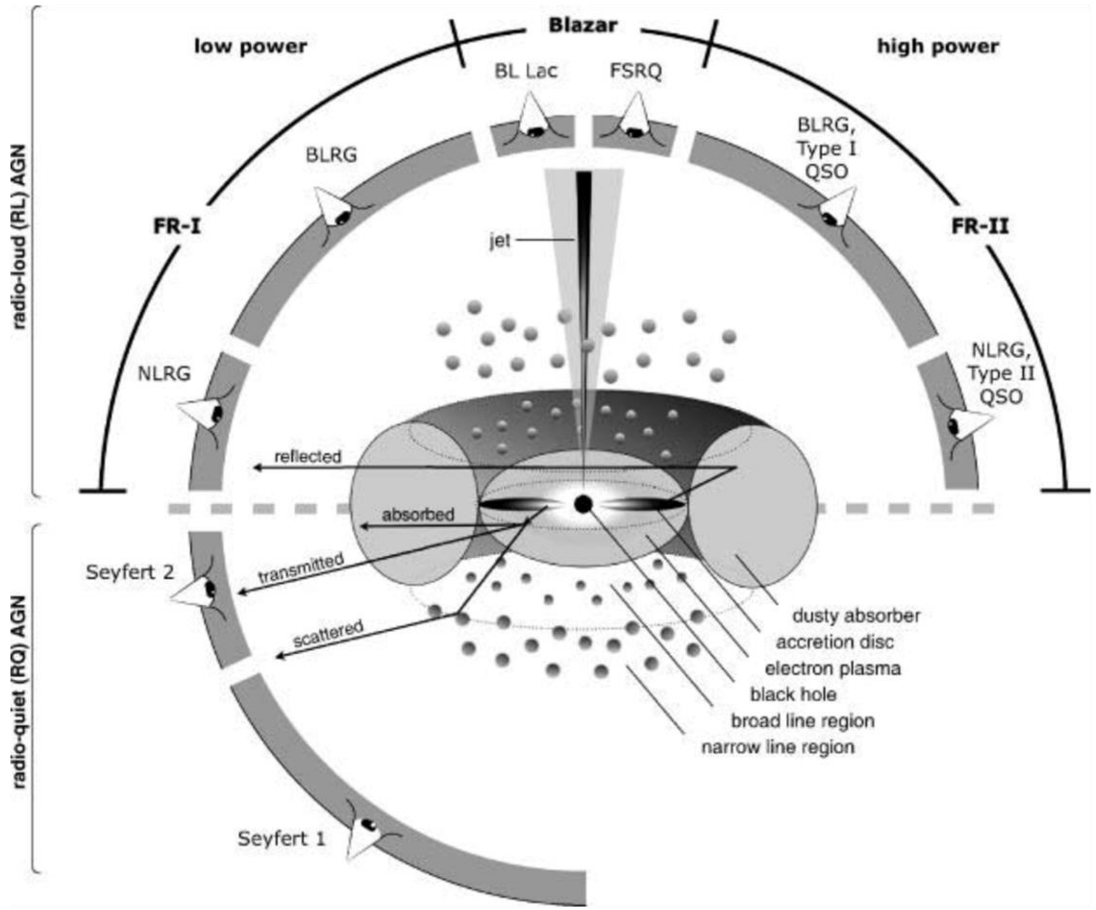

Beckmann and Shrader, 2012, Figure 4.16

Large scale morphology

FR I

- Typically two sided
- Brightness generally decreases with distance from the nucleus
- Lower luminosity

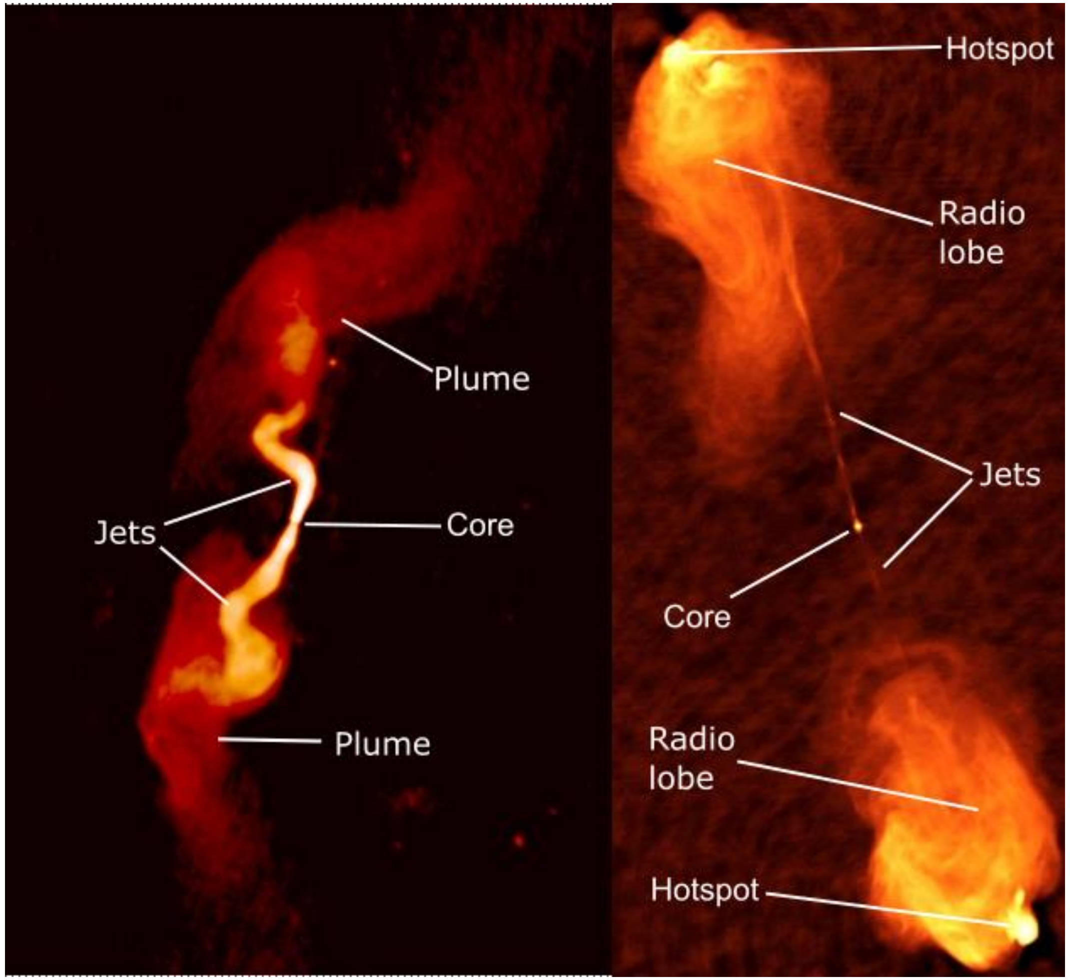

FR II

- Jets can be single or double-sided
- Jet terminates in hotspots with bright lobe
- Higher luminosity

Left: 3C 31, NRAO, see Laing and Bridle(2002b).

Right: Cyg A, NRAO, see Carilli and Barthel (1996).

Large scale morphology

FR I

– Decelerate between parsec-kpc scales

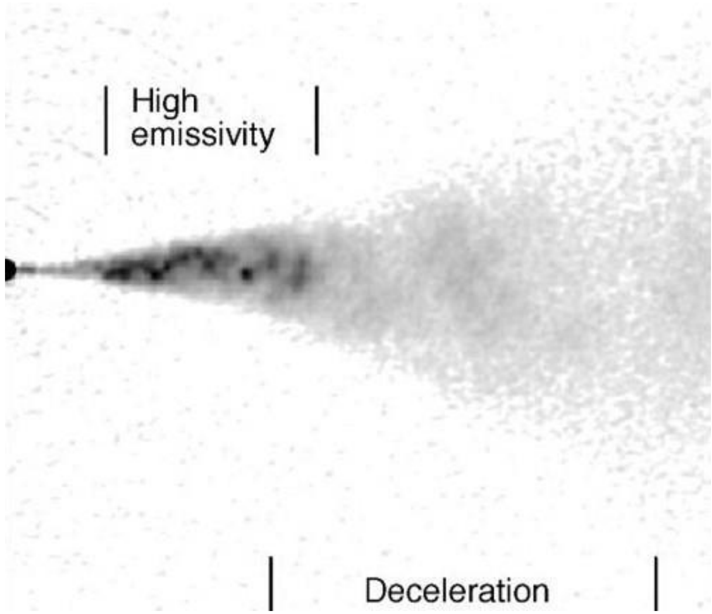

Model for FR I deceleration, Laing and Bridle (2014)

FR II

– Remains relativistic, terminates in a shock

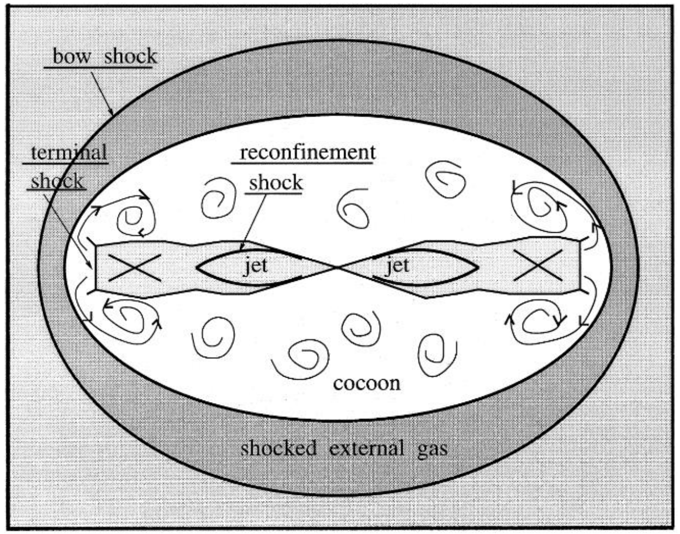

Diagram of the large scale structure of an FR II radio source, Komissarov and Falle (1998).

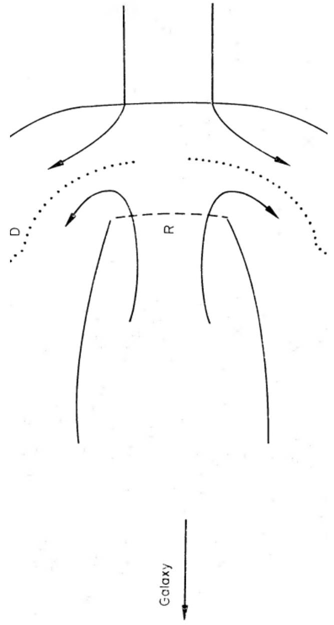

Diagram of flow at terminal shock, Blandford and Rees (1974)

Simulating AGN jets

FR II like morphology

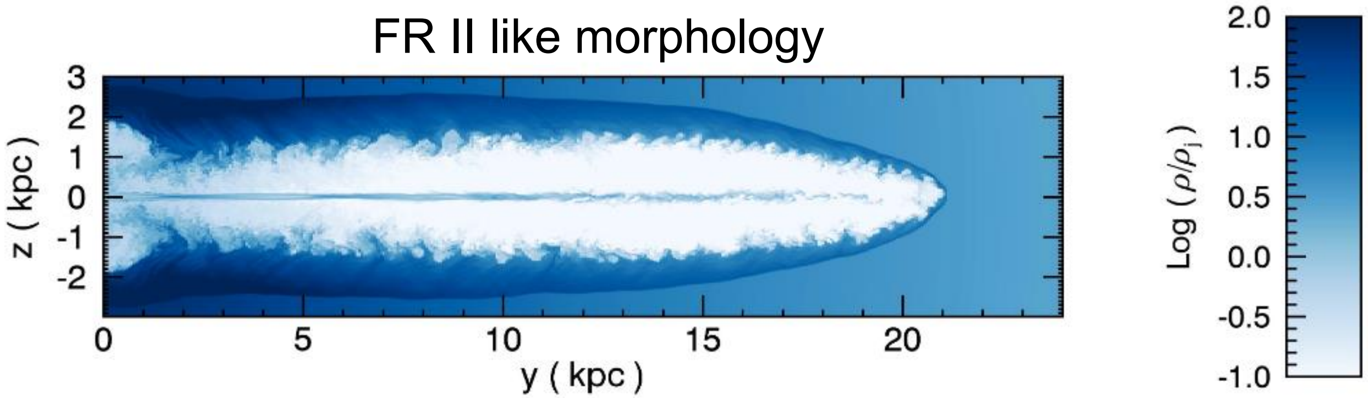

FR I like morphology

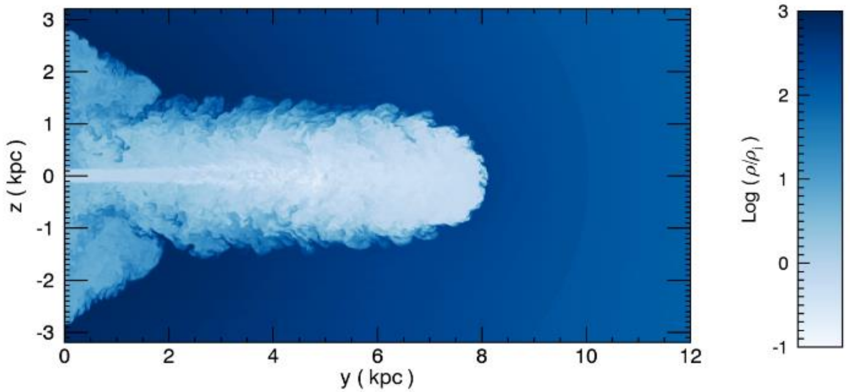

Massaglia, et.al. (2017)

The Morphology and kinematics of AGN jets can be simulated as a thermal fluid.

FR II like morphologies are “easy” to reproduce by injecting supersonic jet into a background region

FR I like structures are more complicated to reproduce.

Massaglia, et.al. (2017) found kinetic luminosities of $\approx 10^{42}$ erg.s^{-1} produced FRI like structures on kiloparsec scales

Deceleration in Jets

Another way to produce FR I type morphologies is through deceleration

This can happen through entrainment of the ambient medium

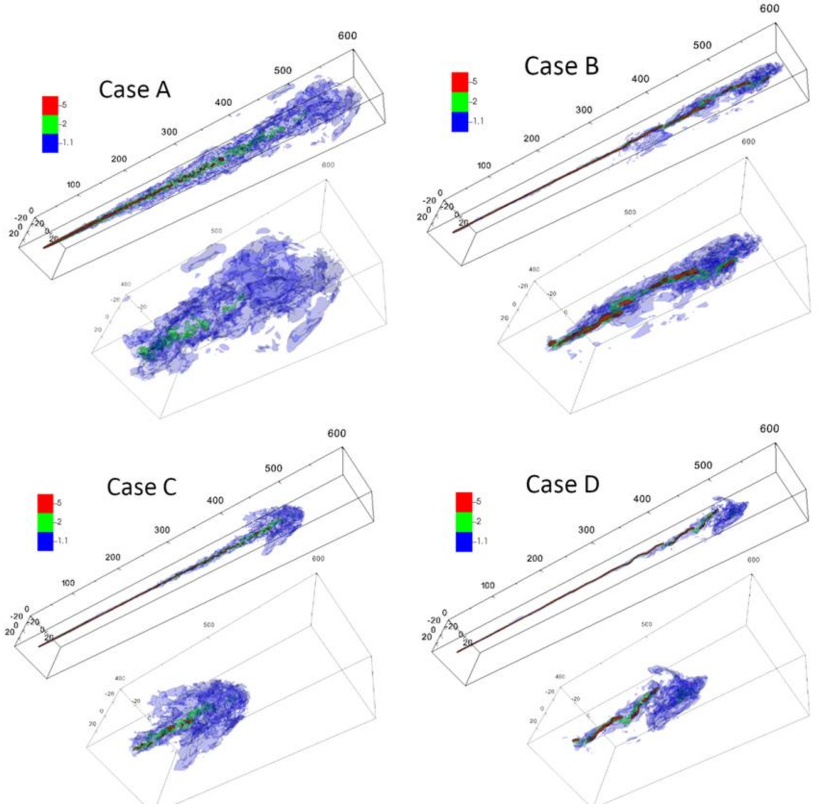

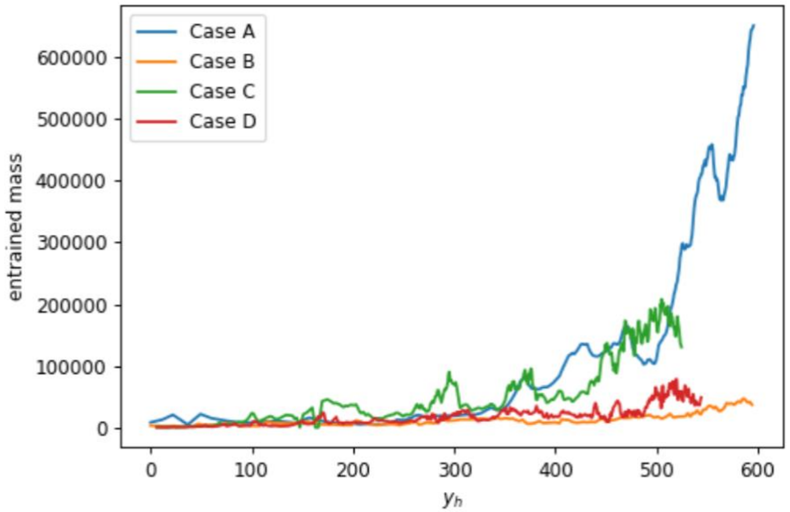

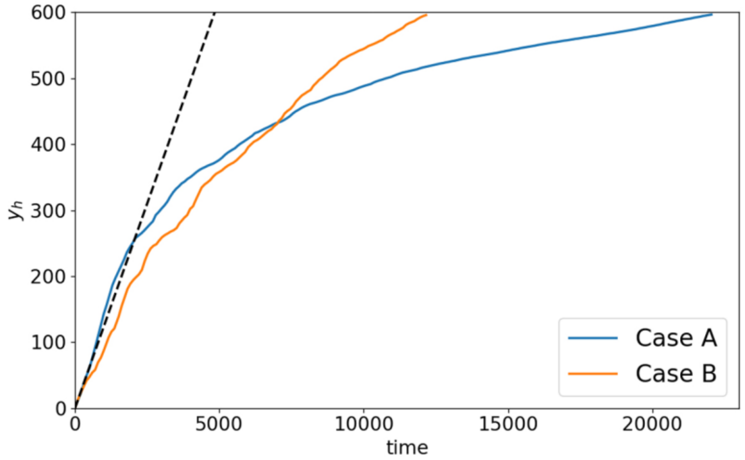

Rossi et. al. (2024)

PLUTO RMHD Simulations

PLUTO v4.4 https://plutocode.ph.unito.it/

- Grid based hydrodynamics code
- Designed for high Mach number flows in astrophysical plasma dynamics
- Opensource

- Lagrangian particles module (Bhargav Vaidya, et. al. ApJ 865:144 (21pp), 2018)
    - Separate particle entities suspended in fluid
    - Represents an ensemble of particles with a finite energy distribution
    - No back reaction on fluid
    - Follow fluid streamlines
    - Energy distribution is evolved with time

$$\frac{d\chi_p}{d\tau} + \frac{\partial}{\partial E}\left[\left(-\frac{E}{3}\nabla_\mu u^\mu + \dot{E}_t\right)\chi_p\right] = 0,$$

- Adiabatic expansion
- Radiative losses
- Diffusive shock acceleration

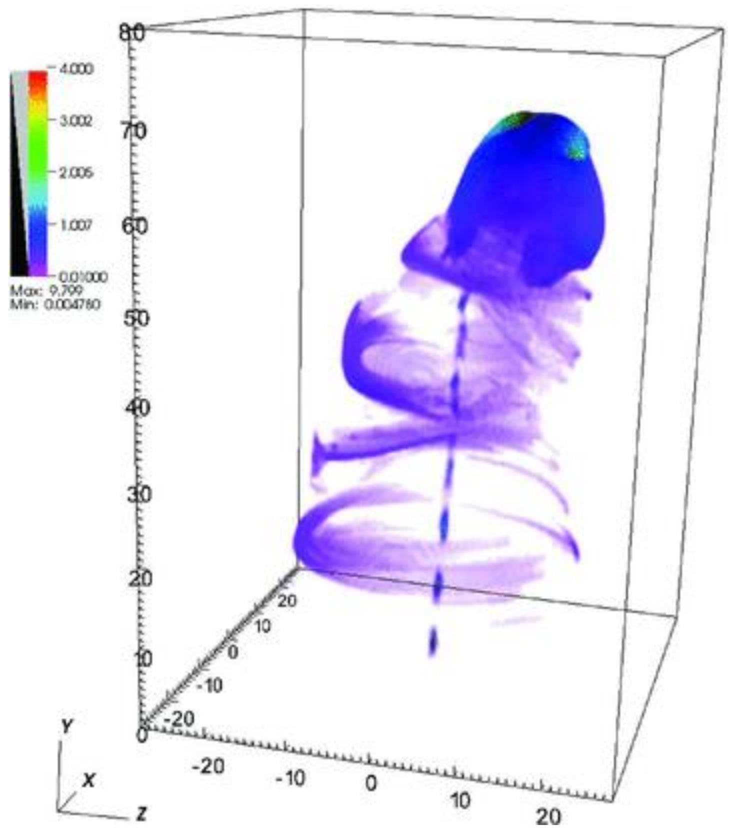

Mignone et. Al., (2010)

Synchrotron Emission

Model the I, Q and U Stokes parameters of the Synchrotron emission

Emission coefficients:

$$j'_I(\nu', \hat{\mathbf{n}}'_{\rm los}) = \frac{\sqrt{3}}{4\pi}\frac{q^3}{m_e c^2}|\mathbf{b}\times\hat{\mathbf{n}}'_{\rm los}|\int n'_e(\gamma')F(x)\mathrm{d}\gamma'.$$

$$j'_{pol}(\nu', \hat{\mathbf{n}}'_{\rm los}) = \frac{\sqrt{3}}{2\pi}\frac{q^3}{m_e c^2}\mathbf{b}\times\hat{\mathbf{n}}'_{\rm los}|\int n'_e(\gamma')G(x)\mathrm{d}\gamma'.$$

$$j_Q = j_{pol}\cos 2\chi$$
$$j_U = j_{pol}\sin 2\chi,$$

Absorption coefficients:

$$\alpha_I(\nu', \hat{\mathbf{n}}'_{\rm los}) = -\frac{\sqrt{3}}{8\pi}\frac{q^3}{m_e^2 c^2\nu^2}|\mathbf{b}\times\hat{\mathbf{n}}'_{\rm los}|\int \gamma^2\frac{\partial}{\partial\gamma}\left[\frac{n'_e(\gamma')}{\gamma^2}\right]F(x)\,\mathrm{d}\gamma'\mathrm{d}\Omega'_\tau.$$

$$\alpha_{pol}(\nu', \hat{\mathbf{n}}'_{\rm los}) = -\frac{\sqrt{3}}{8\pi}\frac{q^3}{m_e^2 c^2\nu^2}|\mathbf{b}\times\hat{\mathbf{n}}'_{\rm los}|\int G(x),\gamma^2\frac{\partial}{\partial\gamma}\left[\frac{n'_e(\gamma')}{\gamma^2}\right]\mathrm{d}\gamma'\mathrm{d}\Omega'_\tau.$$

$$\alpha_Q = \alpha_{pol}\cos 2\chi$$
$$\alpha_U = \alpha_{pol}\sin 2\chi,$$

Lorentz transformations: $j_I(\nu, \hat{\mathbf{n}}_{\rm los}) = \delta_D^2 j'_I(\nu', \hat{\mathbf{n}}'_{\rm los}),$ $\alpha_I(\nu, \hat{\mathbf{n}}_{\rm los}) = \delta_D^{-1}\alpha'_I(\nu', \hat{\mathbf{n}}'_{\rm los}).$

Emission: Radiative transfer

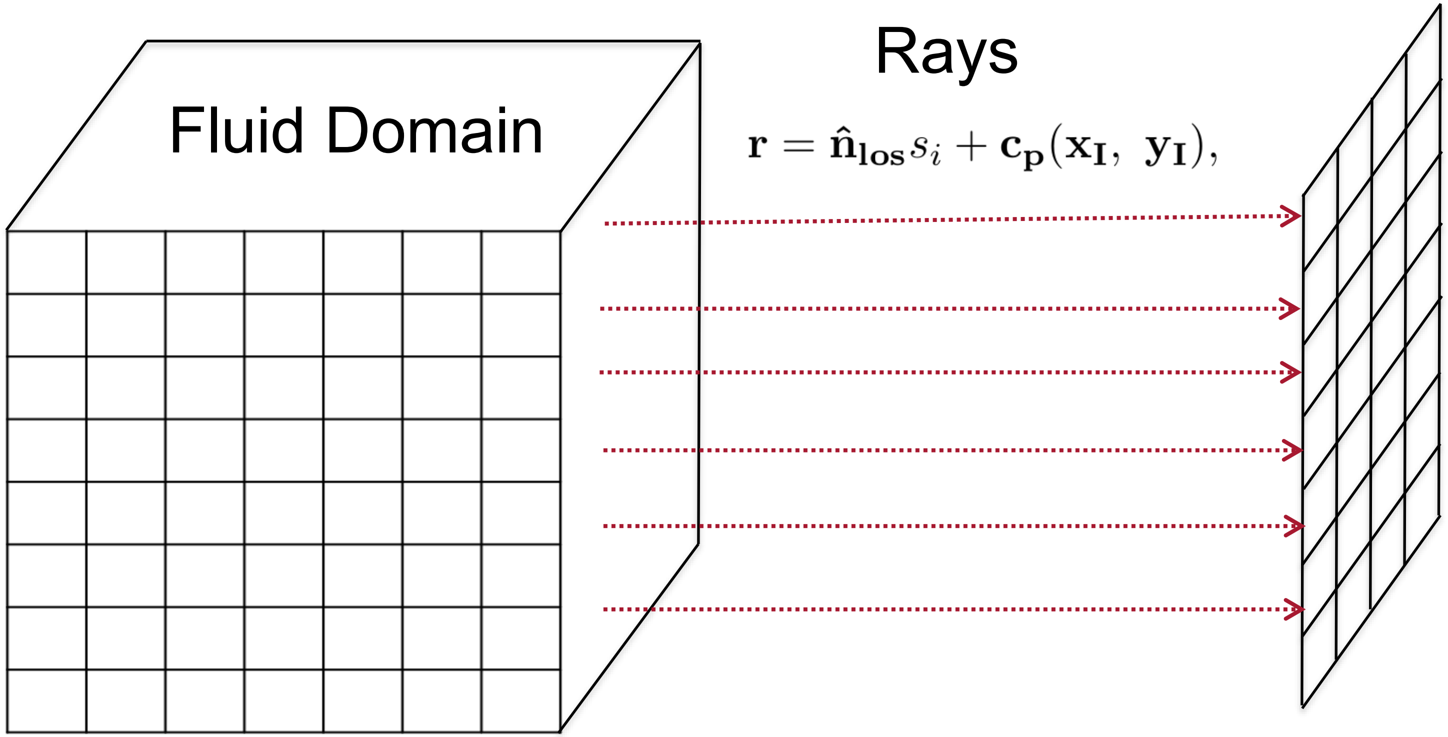

$$\mathbf{r} = \hat{\mathbf{n}}_{\mathbf{los}} s_i + \mathbf{c_p}(\mathbf{x_I},\ \mathbf{y_I}),$$

Image

$$\begin{aligned} \hat{\mathbf{n}}_{\mathbf{los}} &= (\sin\theta\cos\phi\hat{\mathbf{x}},\ \sin\theta\sin\phi\hat{\mathbf{y}},\ \cos\theta\hat{\mathbf{z}}). \\ \hat{\mathbf{x}}_{\mathbf{I}} &= (-\sin\phi\hat{\mathbf{x}},\ \cos\phi\hat{\mathbf{y}},\ 0\hat{\mathbf{z}}) \\ \hat{\mathbf{y}}_{\mathbf{I}} &= (-\cos\phi\cos\theta\hat{\mathbf{x}},\ -\sin\phi\cos\theta\hat{\mathbf{y}},\ \sin\theta\hat{\mathbf{z}}). \end{aligned}$$

Accounting for light travel time

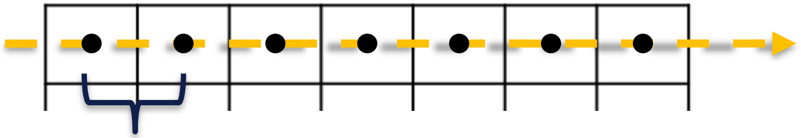

$$\Delta s = c\Delta t$$

$$\mathbf{r} = \hat{\mathbf{n}}_{\mathbf{los}} c t_i + \mathbf{c_p}(\mathbf{x_I},\ \mathbf{y_I}).$$

Emission: Radiative transfer

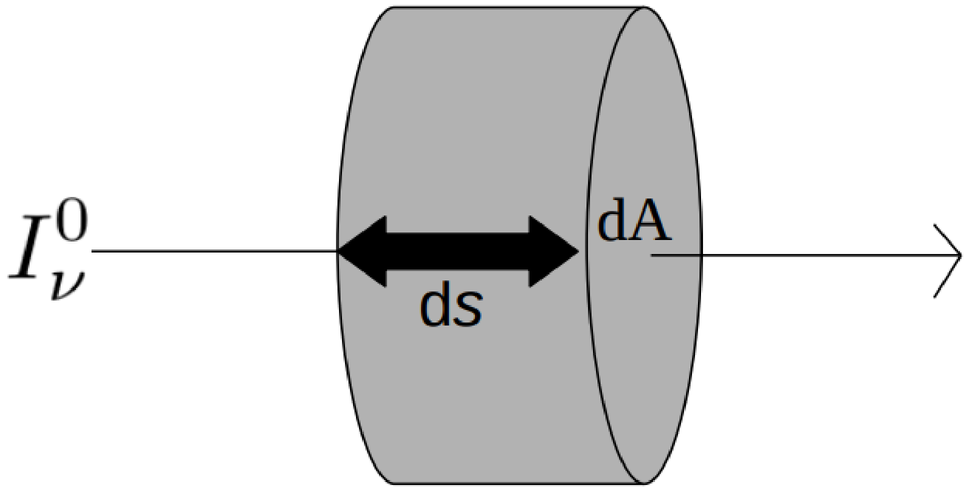

$$\frac{dI_S}{ds} = J_S - M_{ST} I_S,$$

$$\frac{d}{ds}\begin{bmatrix} I \\ Q \\ U \end{bmatrix} = \begin{bmatrix} j_I \\ j_Q \\ j_U \end{bmatrix} - \begin{bmatrix} \alpha_I & \alpha_Q & \alpha_U \\ \alpha_Q & \alpha_I & 0 \\ \alpha_U & 0 & \alpha_I \end{bmatrix} \begin{bmatrix} I \\ Q \\ U \end{bmatrix}.$$

Integration of radiative transfer equation along the path of the ray

$$\int \frac{dI(\mathbf{x_I},\ \mathbf{y_I})}{ds} ds \approx \sum_{i=0}^{i=N} \frac{dI(\mathbf{x_I},\ \mathbf{y_I})}{ds} \Delta s,$$

The integration is split for optically thick and thin regimes

$$I_{S[i]} = \begin{cases} I_{S[i-1]} + \left[J_{S[i]} - M_{ST[i]} I_{S[i-1]}\right] c\Delta t, & \Delta\tau_I < 1, \\ S_{S[i]}(1 - e^{-\Delta\tau_I}) + \Lambda_{\alpha[i]} I_{S[i-1]} e^{-\Delta\tau_I}, & \Delta\tau_I > 1. \end{cases}$$

Where,

$$S_i = \frac{J_i}{\alpha_i}, \qquad \tau = \alpha\Delta s$$

RMHD Simulations

Three scenarios, with different velocities

- Relativistic jet: $\Gamma = 10$
- Mildly relativistic jet: $\Gamma = 1.2$
- Non-relativistic jet: $\Gamma = 1.014$

Simulation	**Relativistic**	**Mildly relativistic**	**Non-relativistic**
Resolution [pc]	25	25	25
Lorentz factor (Γ)	10	1.2	1.014
Mach number (M)	30	17	5
Density ratio (η)	10^{-4}	10^{-4}	10^{-3}
Propagation velocity (V_{WS})	0.904	0.301	0.0833
Kinetic luminosity (E_{kin}) [erg.s^{-1}]	10^{47}	10^{44}	10^{43}
Magnetic field ($B_0,\ B_1,\ B_c$) [$\times 3.8 \times 10^{-5} G$]	1, 1, 0.001	1, 1, 0.001	1, 1, 0.001
Plasma parameter (β_m)	7.7	7.7	0.77
Magnetization parameter (σ)	10^{-2}	10^{-2}	10^{-3}
Number of Lagrangian particles	325 550	375 160	299 137

Simulations setup

Domain

- Cartesian computational grid
- Size: 64x64x128 jet radii
- Jet radius ($r_j = 1$ unit ~ 100 pc)

Stationary ambient medium

- Stratified density $\rho(r) = \frac{\rho_a}{1+\left(\frac{r}{40}\right)^2}$

Jet material is injected through a profiled nozzle on the bottom z-boundary

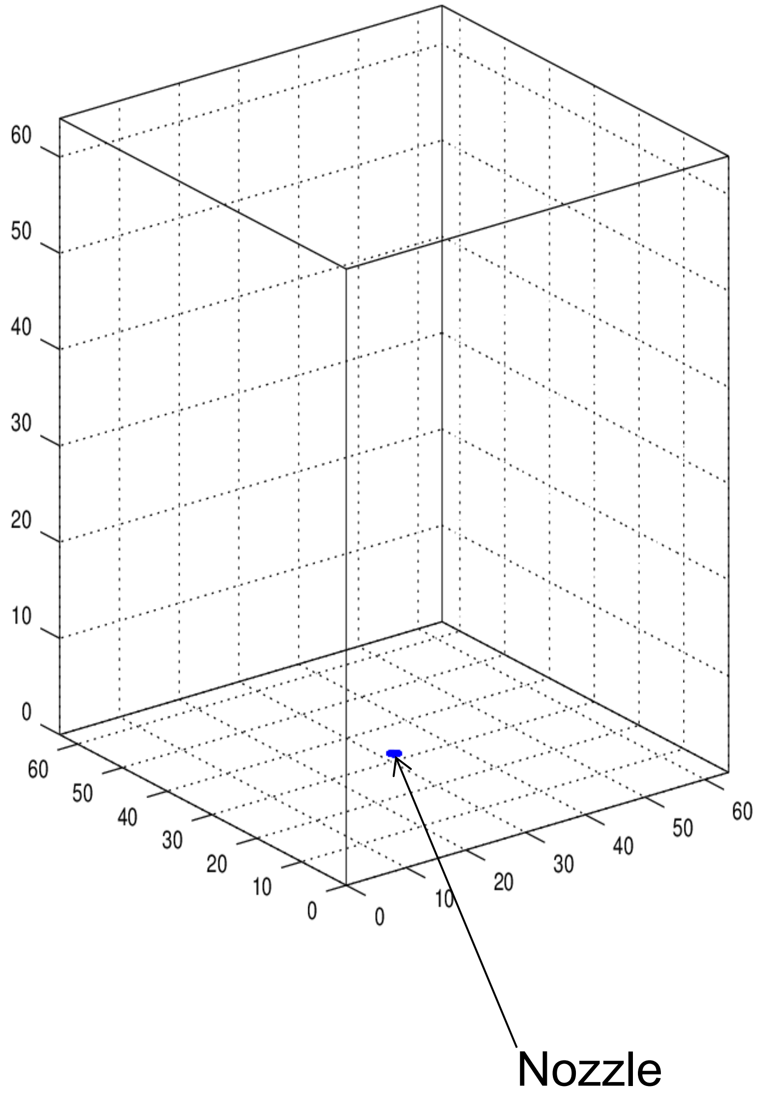

Simulations setup

Domain

- Cartesian computational grid
- Size: 64x64x128 jet radii
- Jet radius ($r_j = 1$ unit ~ 100 pc)

Stationary ambient medium

- Stratified density $\rho(r) = \frac{\rho_a}{1+\left(\frac{r}{40}\right)^2}$

Jet material is injected through a profiled nozzle on the bottom z-boundary

$$B_r = 2B_0 \frac{r_j}{z_j} \frac{\left(\frac{z}{z_j}\right)^3 \tanh\left(\frac{z}{z_j}\right)^4 \tanh\left(\frac{r}{r_j}\right)^2}{\frac{r}{r_j} \cosh\left(\frac{z}{z_j}\right)^4}$$

$$B_z = B_c + \frac{B_0}{\cosh^2\left(\frac{r}{r_j}\right)^2 \cosh\left(\frac{z}{z_j}\right)}$$

$$B_\phi = \begin{cases} B_1 \tanh\left(\frac{r}{5}\right) & \text{for} \quad r \leq r_j, \\ 0 & \text{for} \quad r > r_j \end{cases}$$

$$v_\phi = \frac{B_\phi}{\sqrt{\rho_j}}, \qquad \text{and,}$$

$$v_z = \sqrt{1 - \frac{1}{\Gamma_z^2}},$$

RMHD simulations

2D slices of the simulations through the xz-plane

Relativistic jet

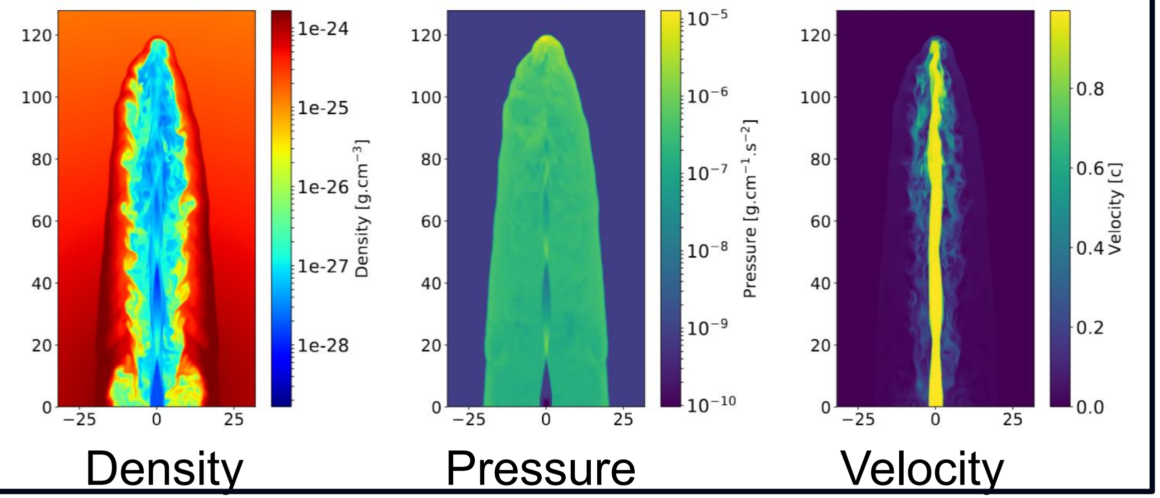

Mildly relativistic jet

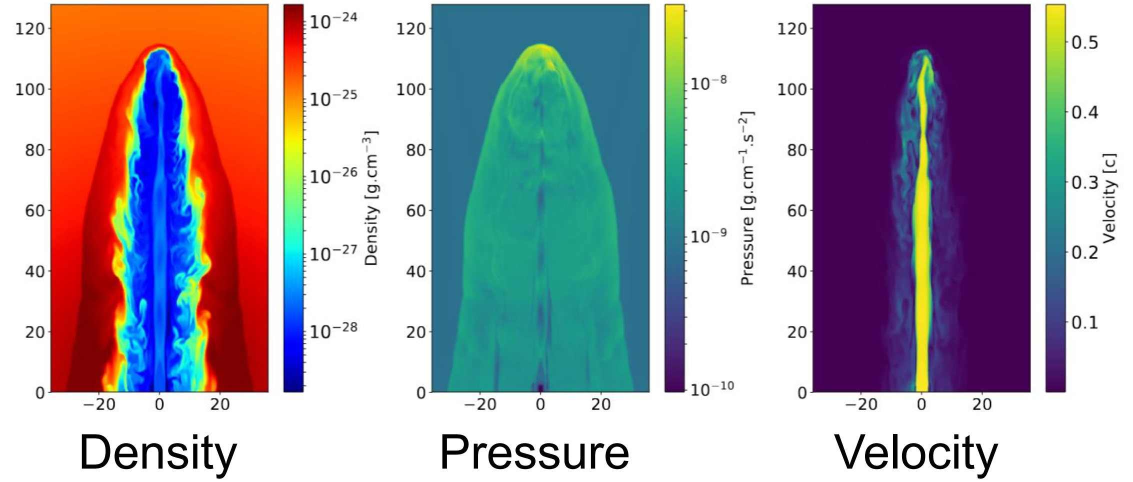

Non-relativistic jet

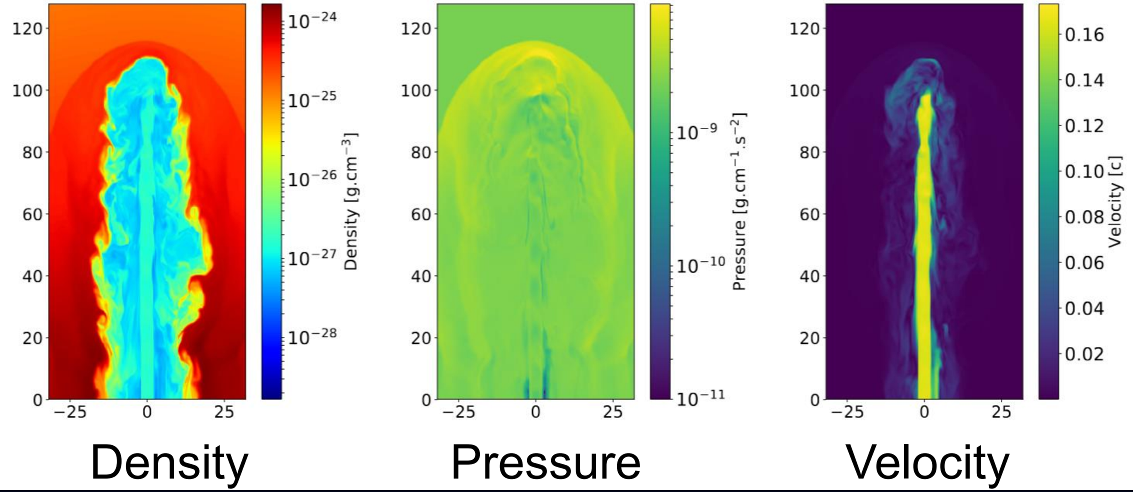

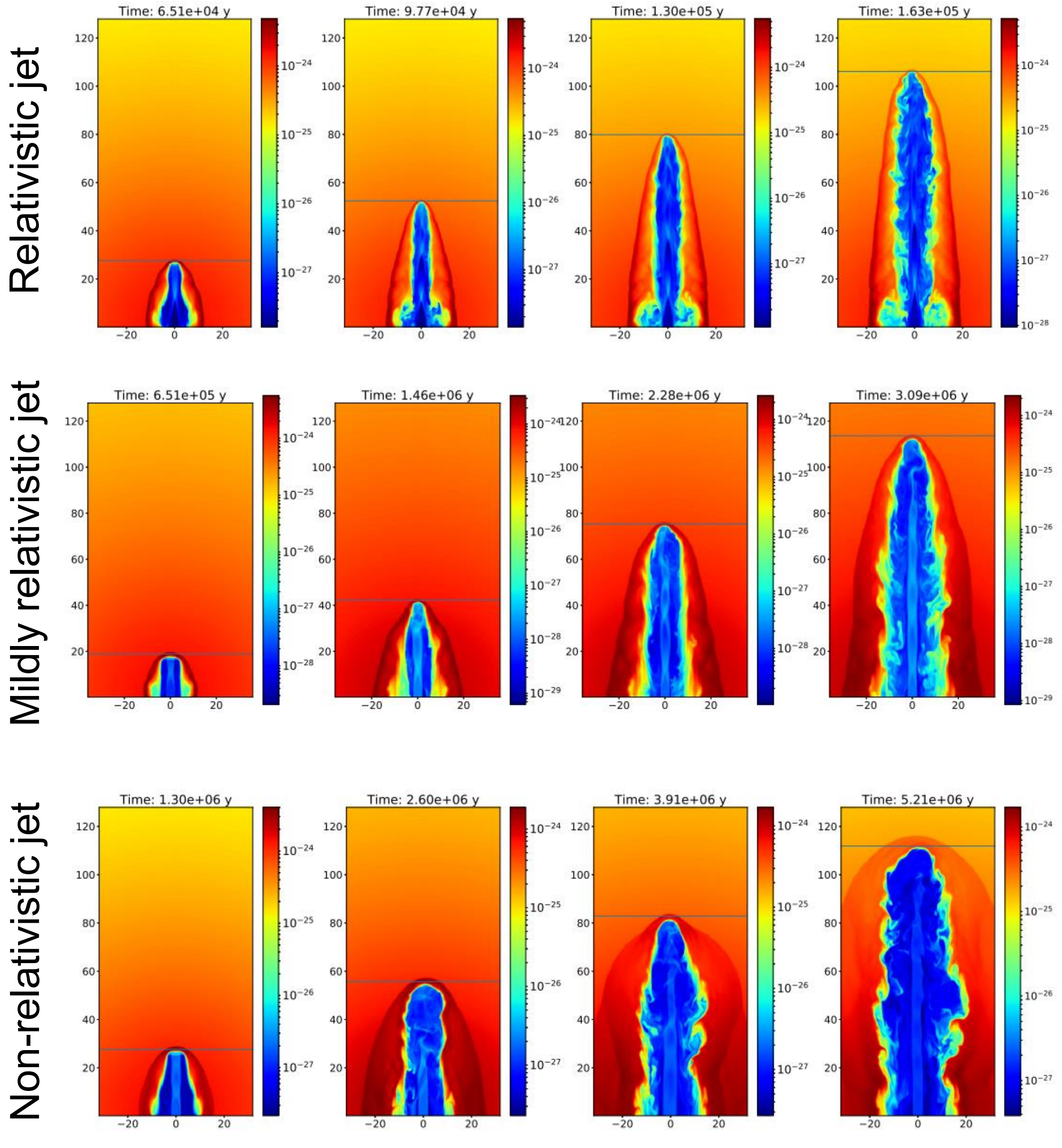

RMHD simulations evolution

Jet propagation
$$V_{\rm ws} = \frac{\sqrt{\eta_R^*}}{1+\sqrt{\eta_R^*}} v_j$$

$$\eta_R^* = \frac{\Gamma^2 \rho_j h_j}{\rho_{\rm am} h_{\rm am}}.$$

Case	Time [y]	Position [100 kpc]	Average velocity [c]	δ_R
Relativistic	6.51×10^4	27.1	0.136	1.43
	9.77×10^4	451.9	0.247	2.02
	1.30×10^5	79.4	0.275	1.71
	1.63×10^5	105.6	0.262	1.31
Mildly relativistic	6.51×10^5	18.1	0.00901	1.35
	1.46×10^6	41.6	0.00940	1.15
	2.28×10^6	74.9	0.0133	1.16
	3.09×10^6	112.4	0.0150	0.915
Non-relativistic	1.30×10^6	26.9	6.72×10^{-3}	1.24
	2.60×10^6	54.9	7.00×10^{-3}	0.963
	3.91×10^6	81.4	6.63×10^{-3}	0.671
	5.21×10^6	111.1	7.44×10^{-3}	0.582

Emission modelling

Lagrangian particles were injected at random positions inside the jet inlet.

- The injection was started after the jet established itself in the domain
- The injection rate was scaled according to mass flux of each simulation

n_e	$10^{-3}\, n_{th}$
γ_{min}	10^2
γ_{max}	10^5
p	2.2

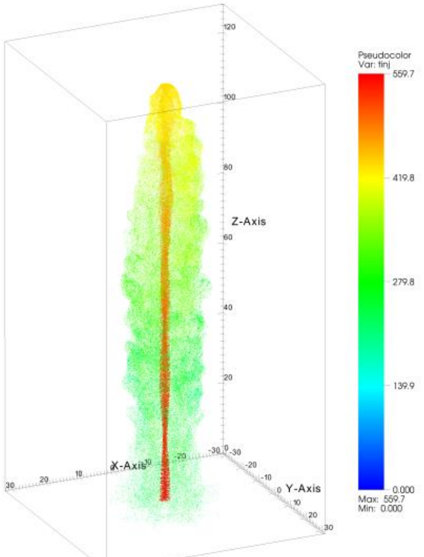

Relativistic jet

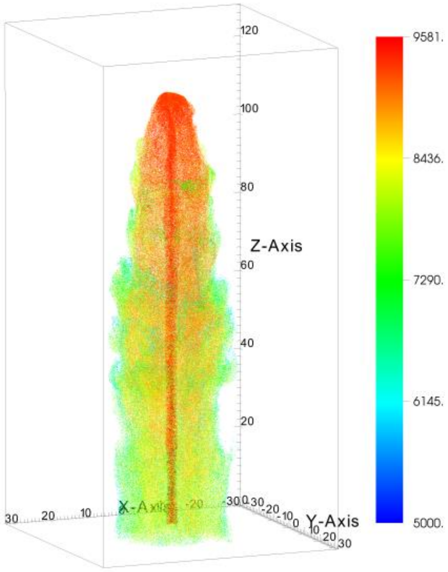

Mildly relativistic jet

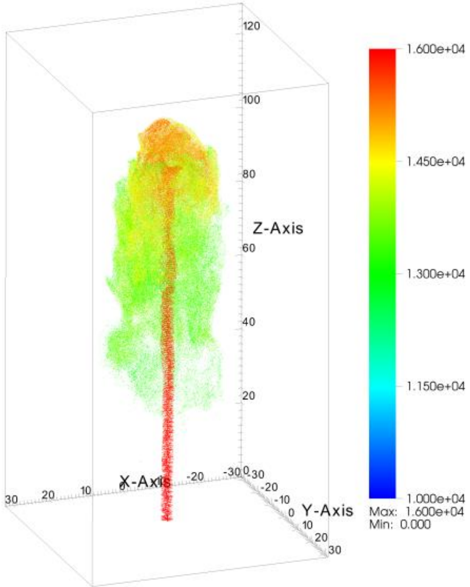

Non-relativistic jet

Intensity maps: 10 GHz, $\theta = 90°$

Intensity maps resemble FR II type radio galaxies for all cases

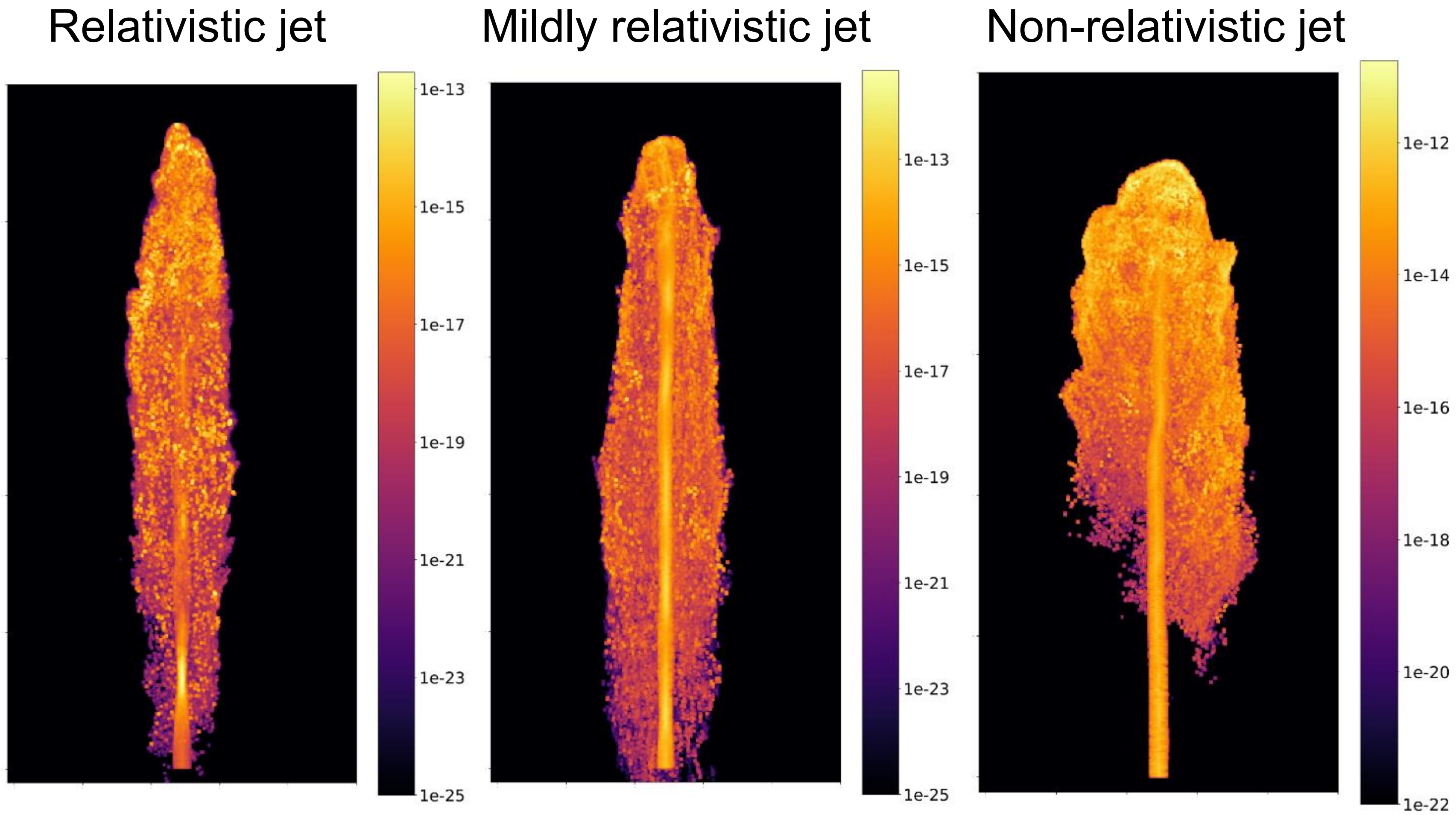

Intensity maps: 10 GHz, $\theta = 90°$

Intensity maps resemble FR II type radio galaxies for all cases

- Jets
  - Stationary emission components

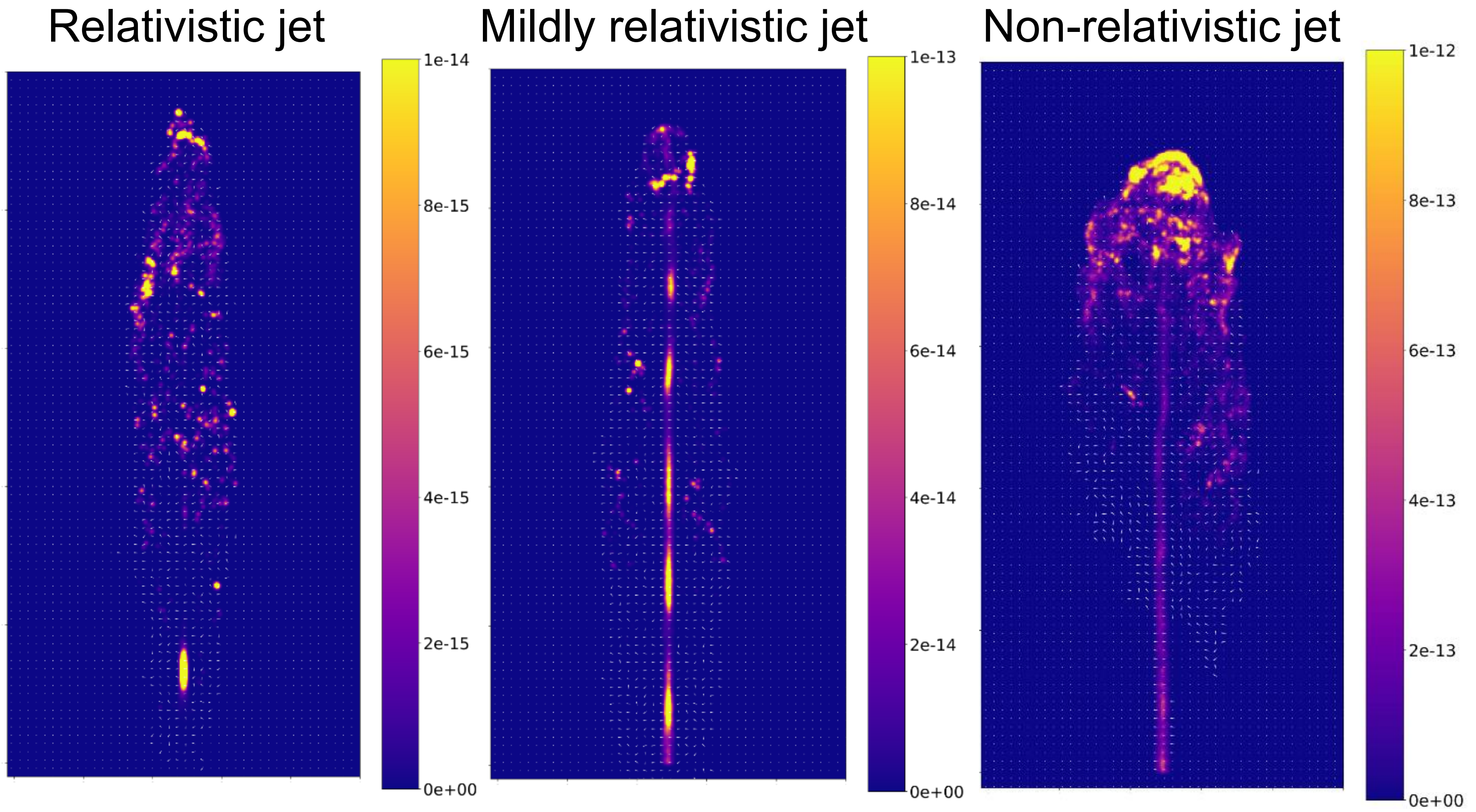

Intensity maps: 10 GHz, $\theta = 90°$

Intensity maps resemble FR II type radio galaxies for all cases

- Jets
  - Stationary emission components
- Lobes
  - Hotspots
  - Filaments

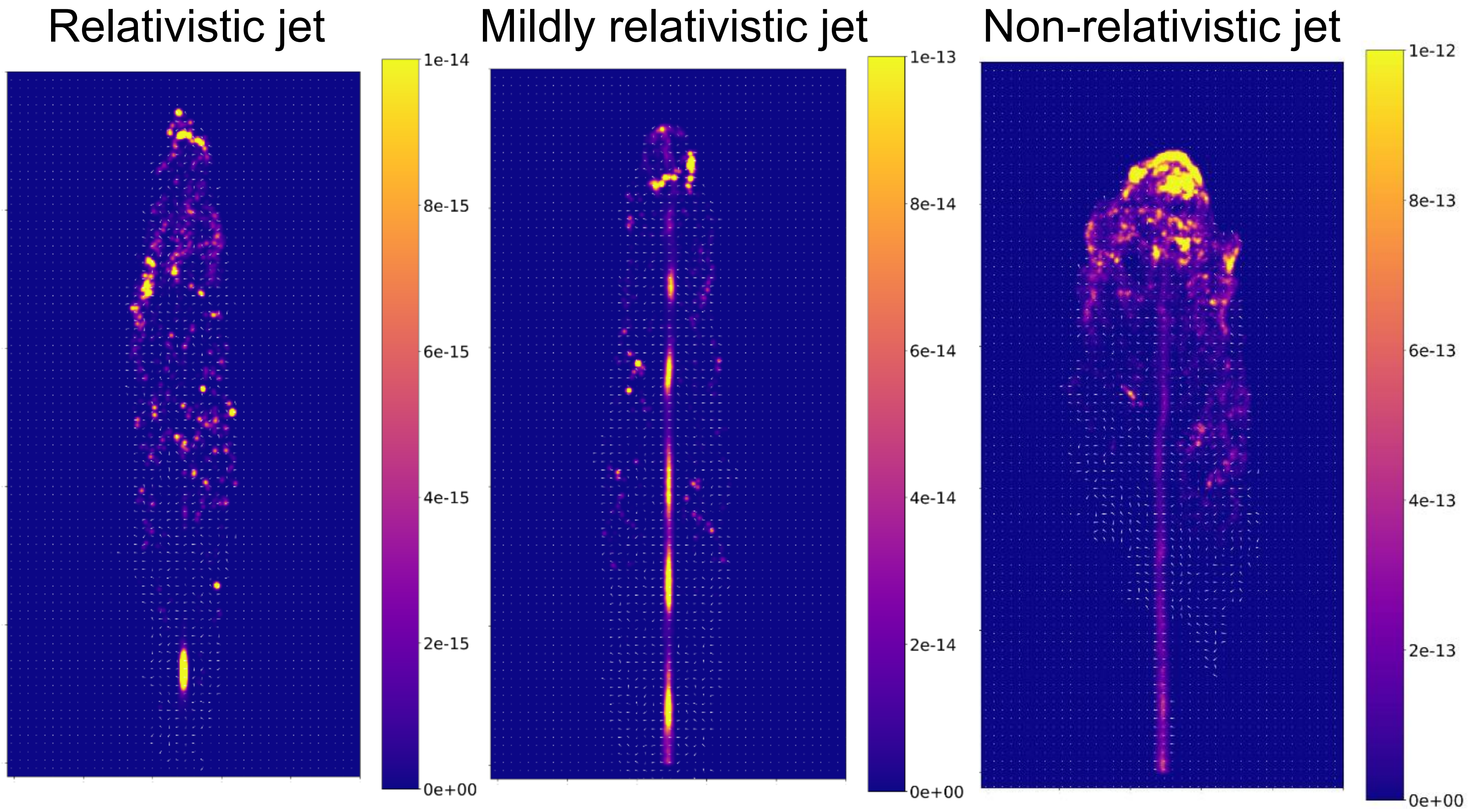

Intensity maps: 10 GHz, $\theta = 90°$

Filaments and hot spots follow magnetic filaments in the lobes

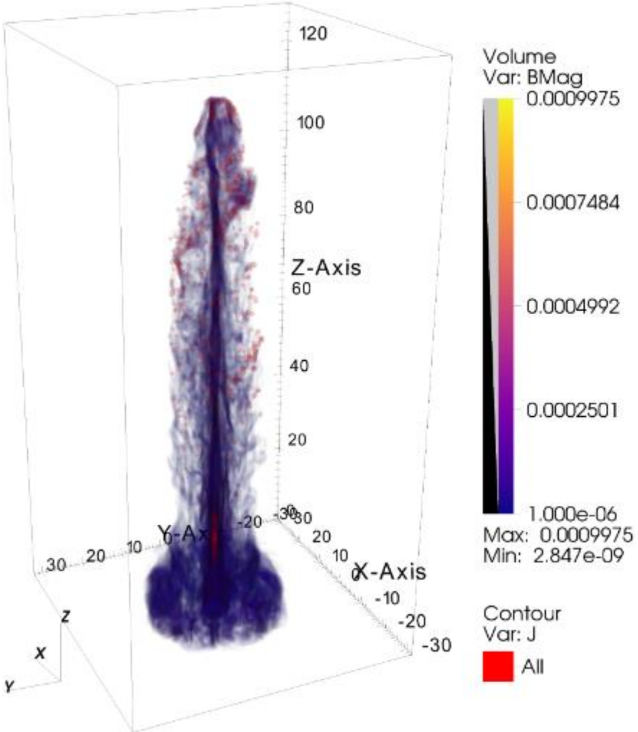

Relativistic jet

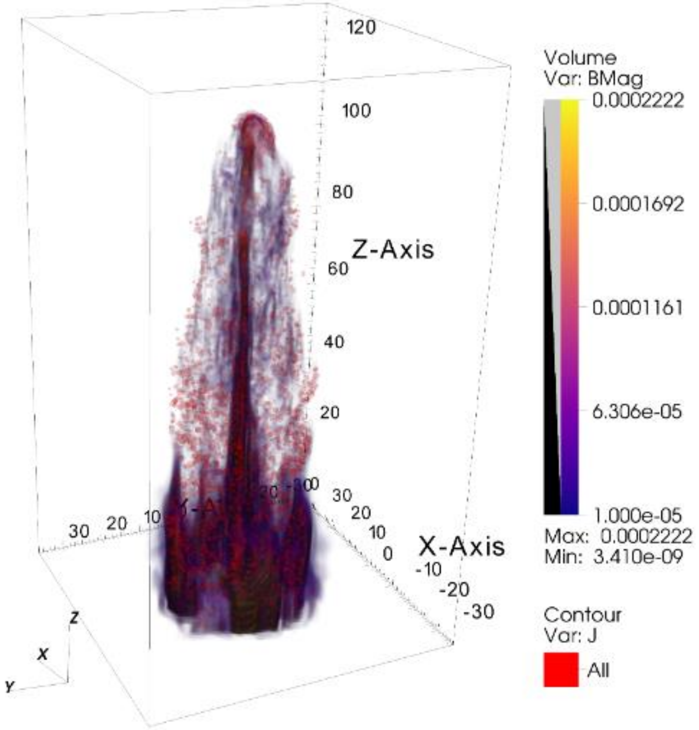

Mildly relativistic jet

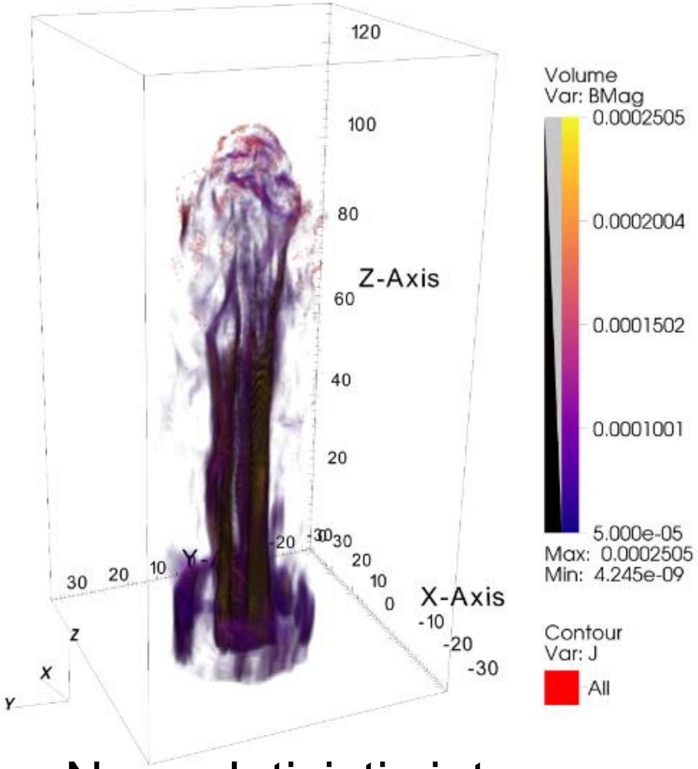

Non-relativistic jet

SED modelling

Relativistic model
Features are dominated by Doppler boosting

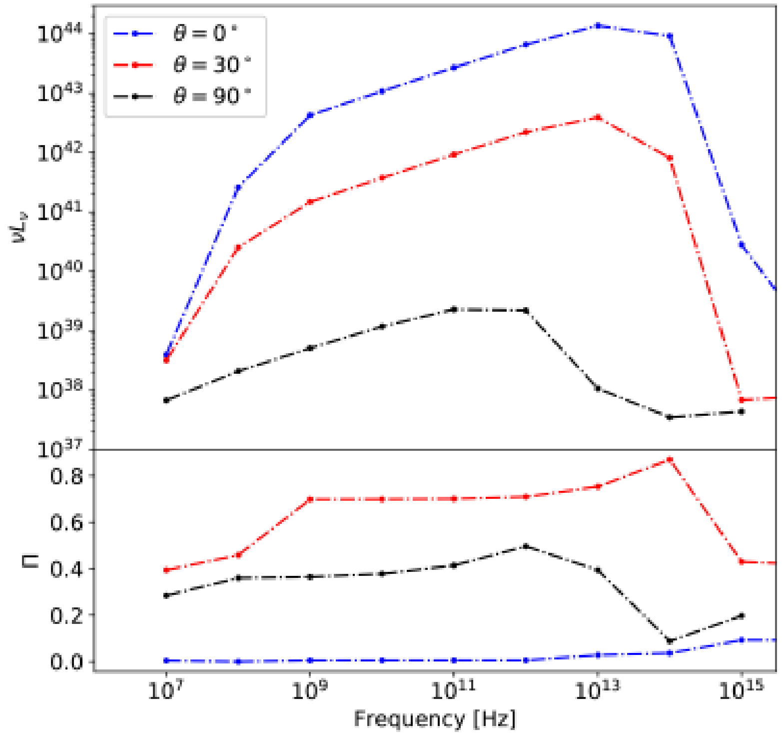

Mildly relativistic model
Magnetic field geometry is important

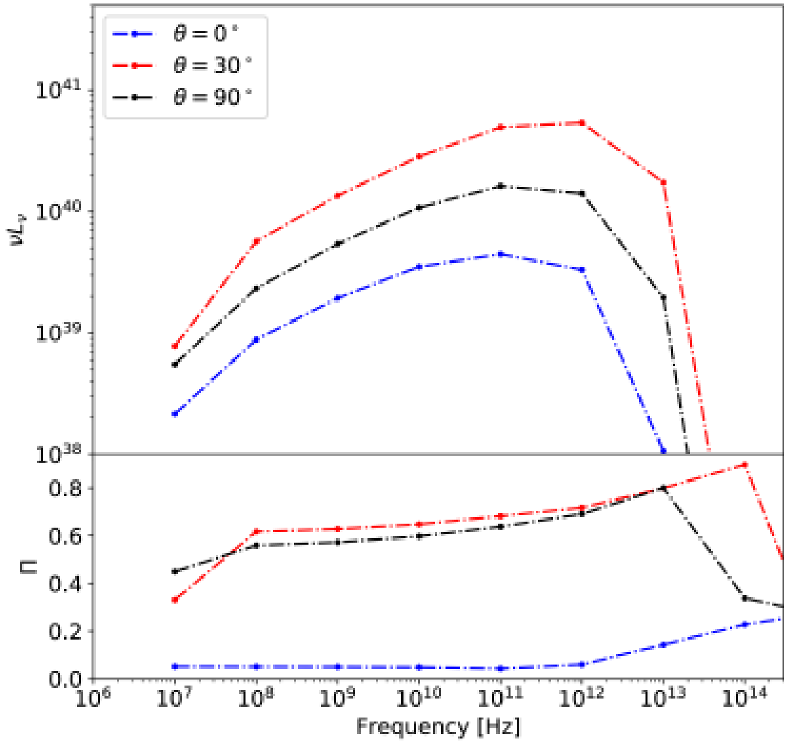

Non-relativistic model
Emission dominated by lobe region

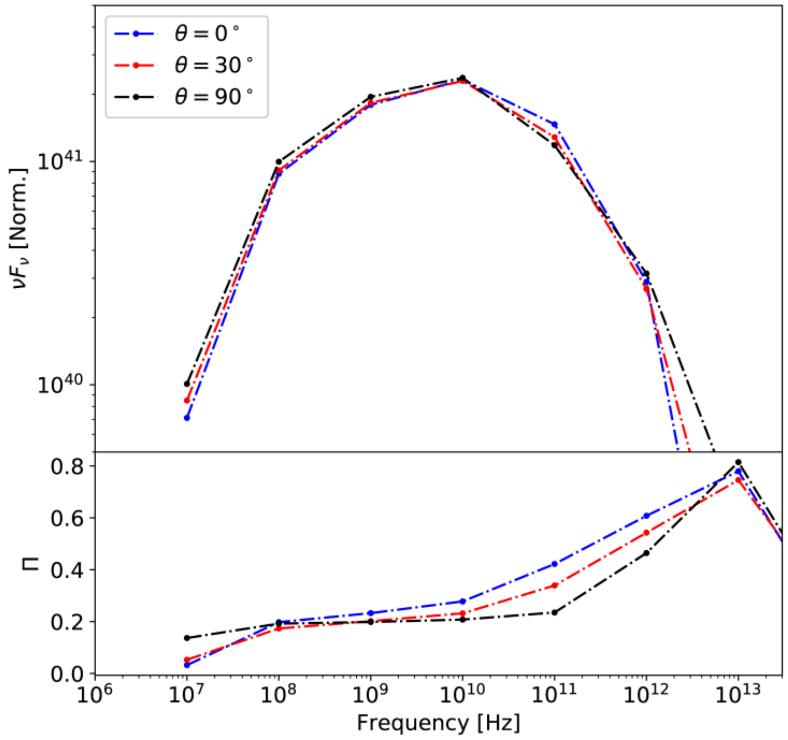

NATURAL AND AGRICULTURAL SCIENCES
UFS

What about FRI's?

For FRI type structure we require deceleration

This can be achieved by a pressure mismatch

Simulation	**Under-pressured jet**
Resolution [pc]	16.6
Lorentz factor (Γ)	1.014
Mach number (M)	5
Density ratio (η)	10^{-3}
Propagation velocity (V_{WS})	0.0051
Kinetic luminosity [erg.s^{-1}]	10^{43}
Magnetic field ($B_0,\ B_1,\ B_c$) [$\times 3.8 \times 10^{-5}$ G]	0.01, 0.04, 0.001
Plasma parameter (β_m)	10^{-4}
Magnetization parameter (σ)	10^{-7}
Number of Lagrangian particles	1 140 765

Decelerated jet

For FRI type structure we require deceleration

This can be achieved by a pressure mismatch

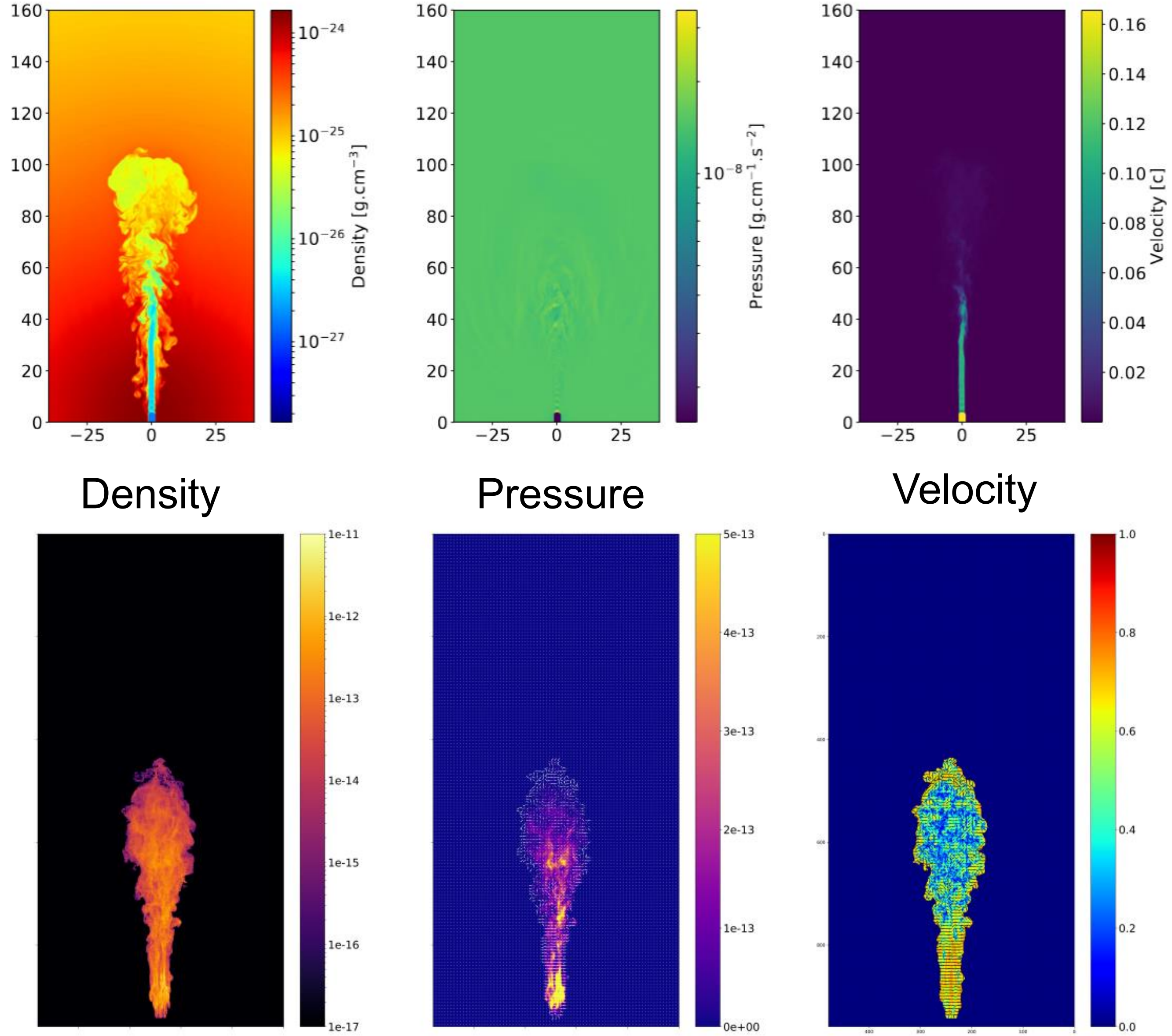

Density Pressure Velocity

Intensity map (log) Intensity map (linear) Polarization

Blazar emission

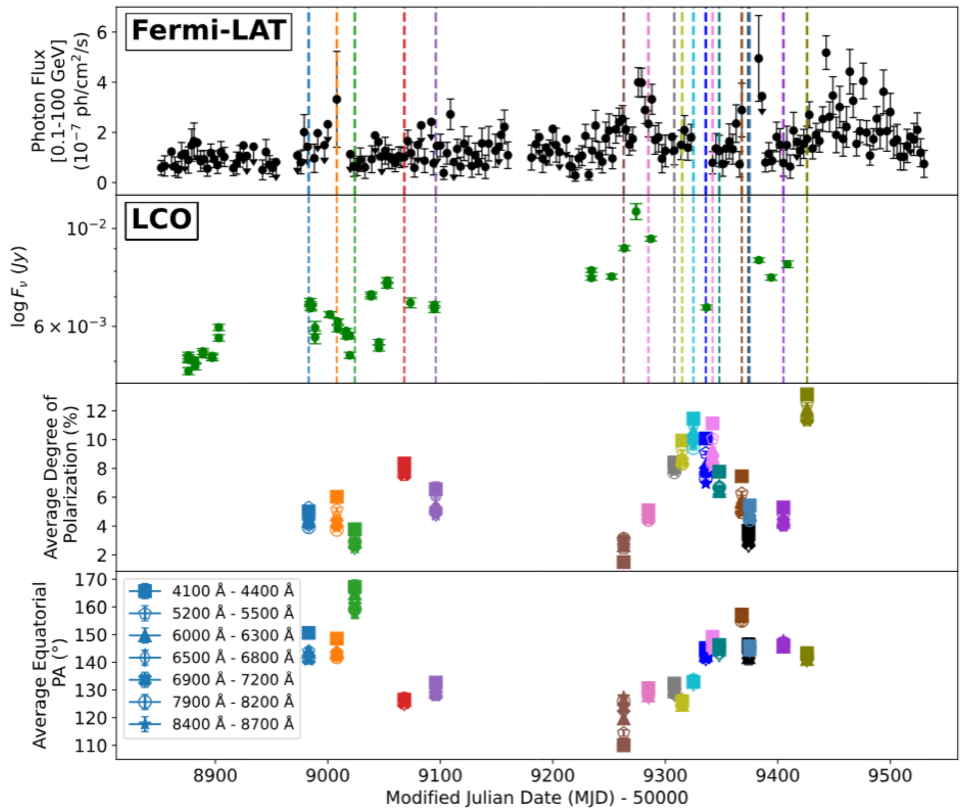

Barnard, et al. (2024). MNRAS, 532, https://doi.org/10.1093/mnras/stae1576

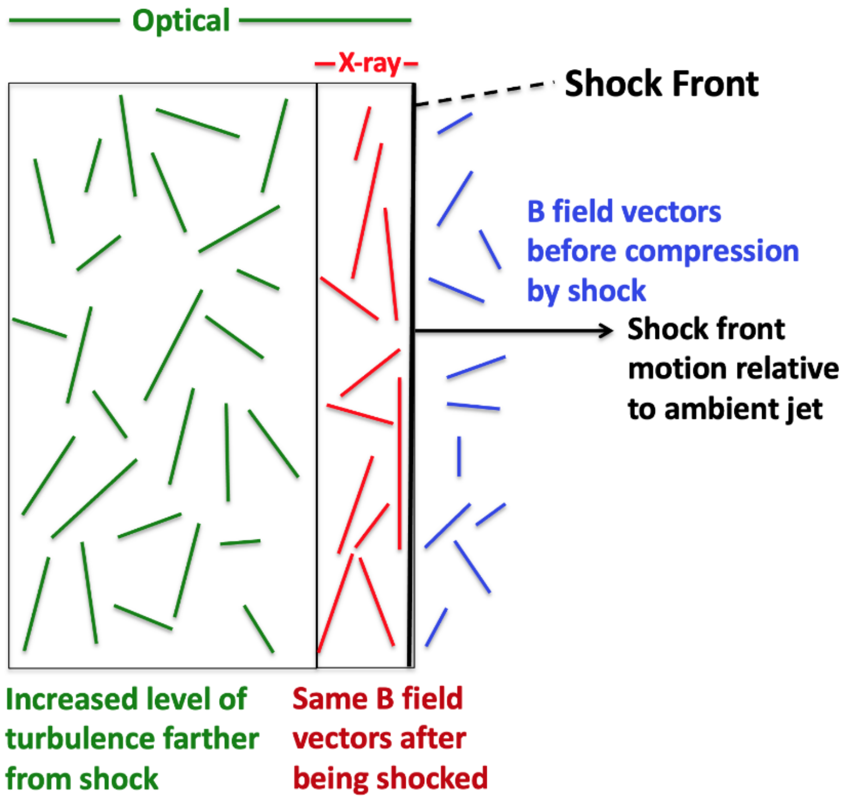

Marscher, A. P., et al. (2024). *Galaxies*, *12*(4), 50. https://doi.org/10.3390/galaxies12040050

Blazar emission

Recent IXPE observations show X-ray polarization is typically higher than Optical (see e.g. Kouch, et. al., 2024)

This is consistent with the shock in jet model (see e.g. Marscher, A. P., et al. 2024).

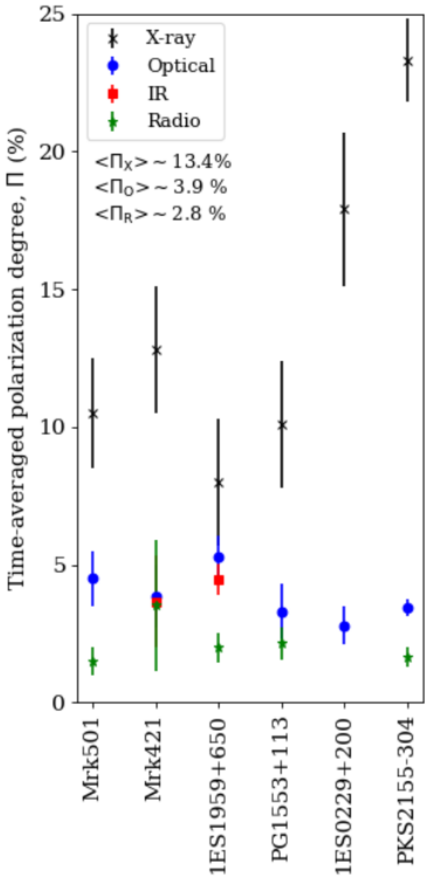

Kouch, et. al., 2024

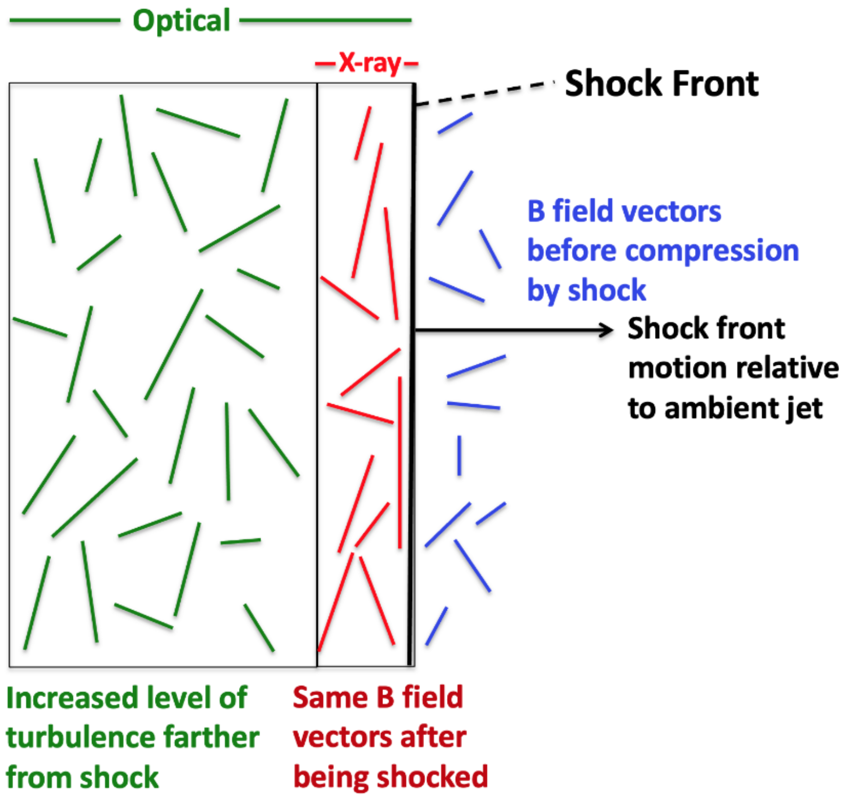

Marscher, A. P., et al. (2024). *Galaxies*, *12*(4), 50. https://doi.org/10.3390/galaxies12040050

Parsec scale Jet model

Initial setup consists of cylindrical jet in a uniform background

Parameter:	Spine:	Sheath:
Lorentz factor (Γ)	10	3
Jet Radius (R)	0.33 pc	1.0 pc
Density ratio (η_ρ)	10^{-3}	10^{-2}
Pressure ratio (η_p)	4.0	2.0
Magnetic field (B)	50 mG	5 mG
Pitch profile parameter (α)	0.5	−2.0

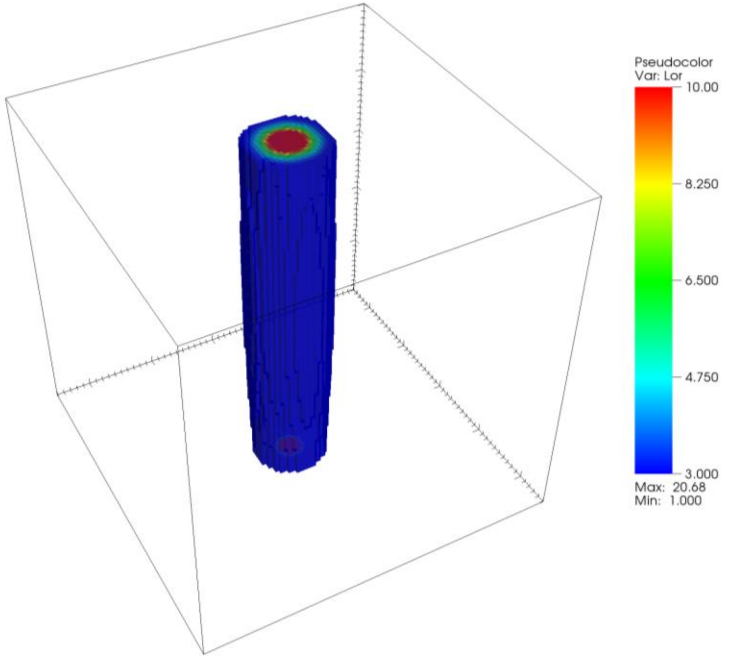

Helical magnetic field :

(Meliani and Keppens, APJ, 705:1594–1606, 2009)

$$B_\phi = \begin{cases} B_{\phi,\mathrm{spine}}\left(\frac{R}{R_{\mathrm{spine}}}\right)^{\alpha_{\mathrm{spine}}/2}; & \text{if } 0 \leq R < R_{\mathrm{spine}} \\ B_{\phi,\mathrm{sheath}}\left(\frac{R}{R_{\mathrm{spine}}}\right)^{\alpha_{\mathrm{sheath}}/2}; & \text{if } R_{\mathrm{spine}} \leq R \leq R_{\mathrm{sheath}} \\ 0; & \text{if } R > R_{\mathrm{sheath}} \end{cases}$$

Jet cross-section

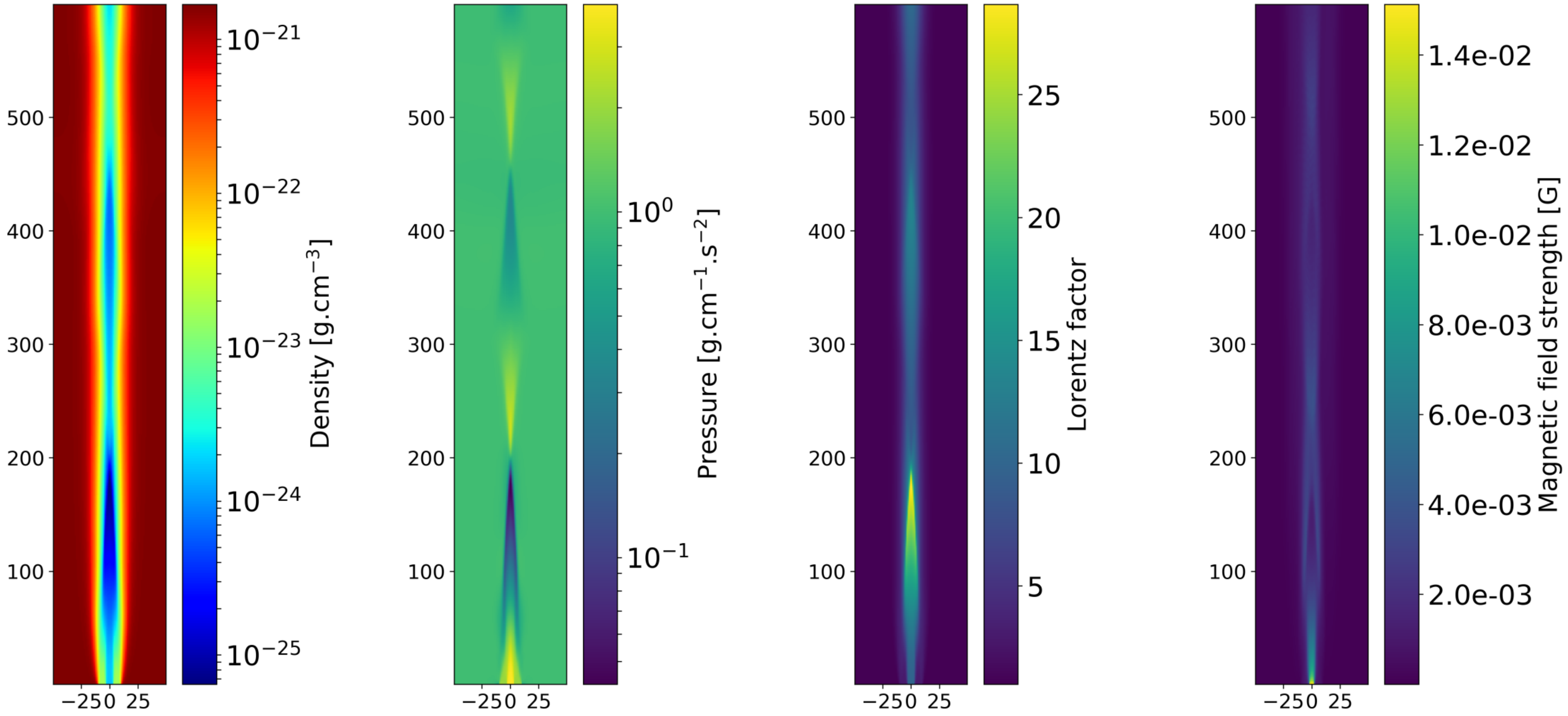

Lagrangian particles

Lagrangian particles were injected at random positions inside the jet inlet.

- The injection was started after the jet established itself in the domain
  - 50 Particles per time step
  - 100 000 Particles total
- Injected with a single power-law distribution

$$n'_{\mathrm{e}}(\gamma') = n'_0 \gamma'^{-p}.$$

- The injection was normalized to 10^{-3} the density of the thermal fluid

γ_{min}	γ_{max}	p
10^2	10^7	5

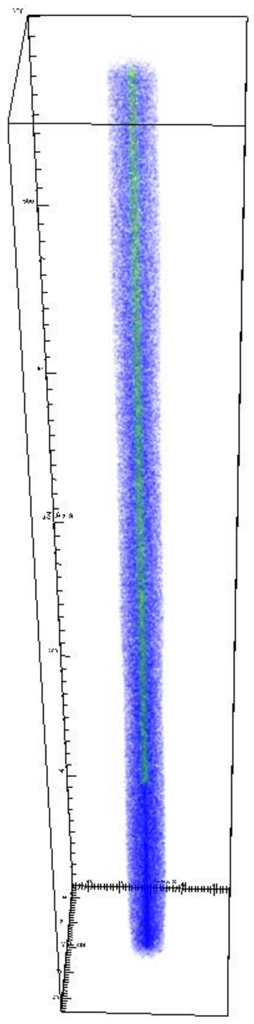

Spatial distribution of particles in simulation

Intensity maps

Different frequencies ($\theta = 30°$)

Radio ($\nu = 10^9$ Hz):
- Entire jet is bright

Optical ($\nu = 10^{14}$ Hz):
- Recollimation shock brighter than jet

X-rays ($\nu = 10^{14}$ Hz):
- Only at recollimation shock

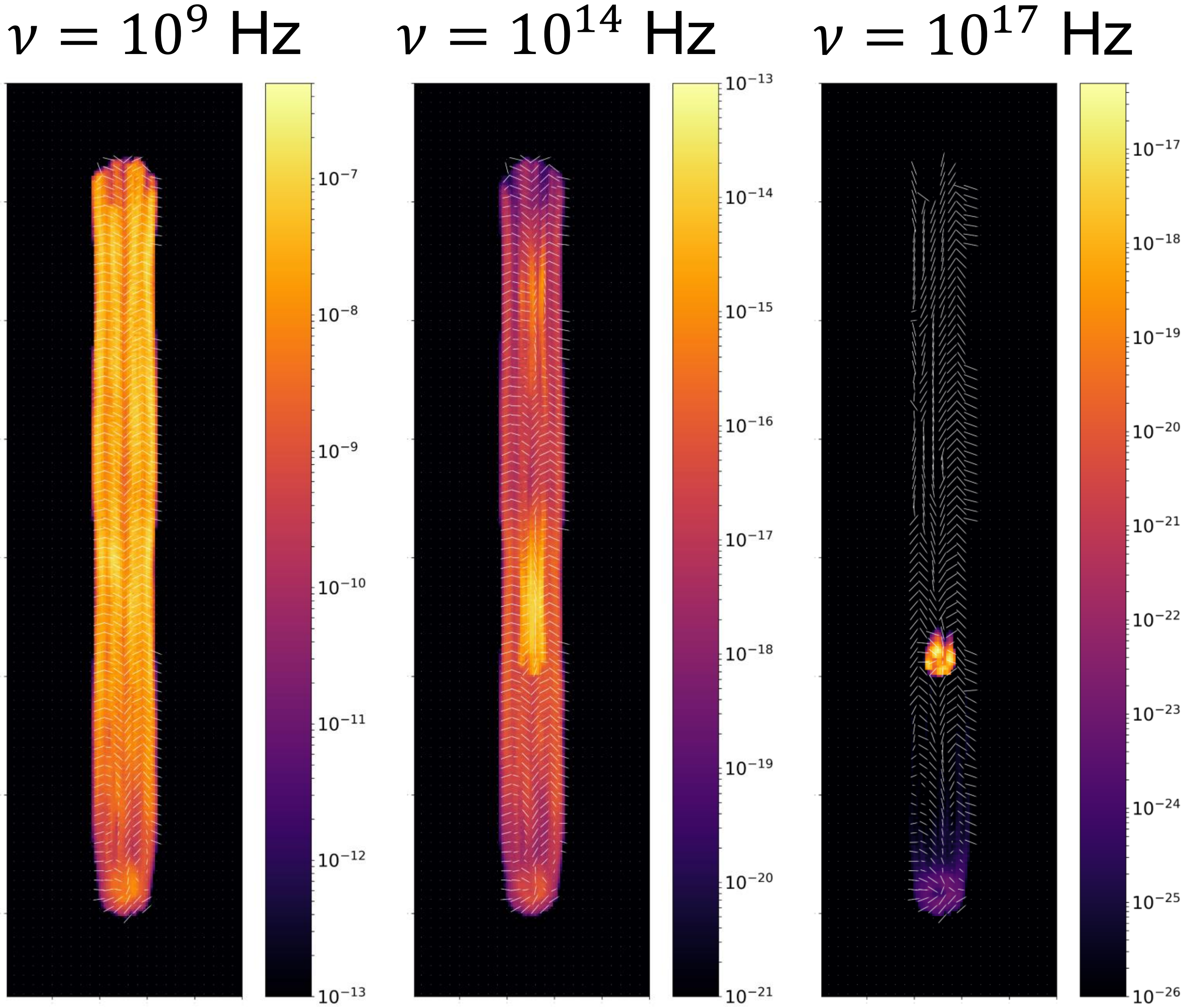

Variability

Variability is simulated through the injection of a region of increased density and magnetic field

ρ	$10^3\ \rho_0$
B	$10\ B_0$
R	$0.5\ R_{spine}$

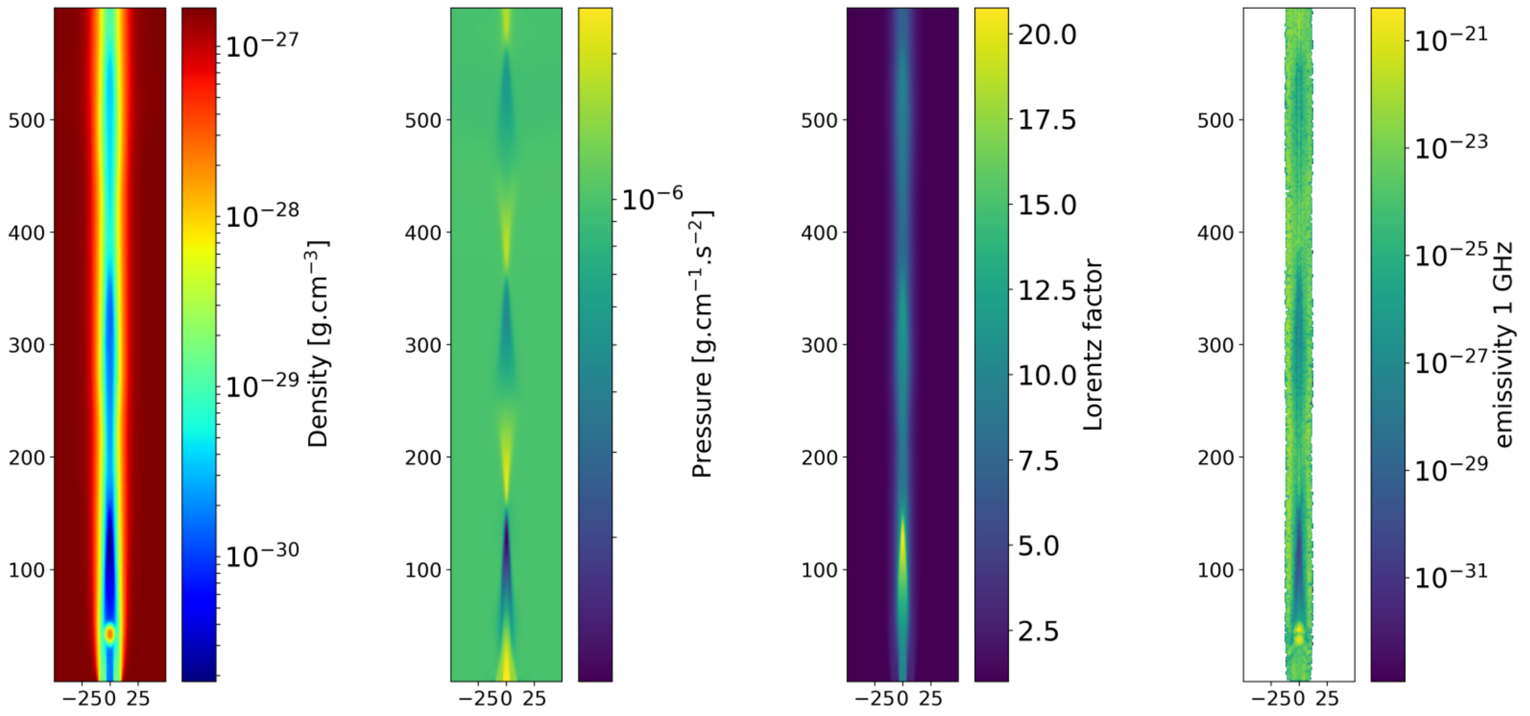

Intensity maps and light curve

$$\theta = 2°$$

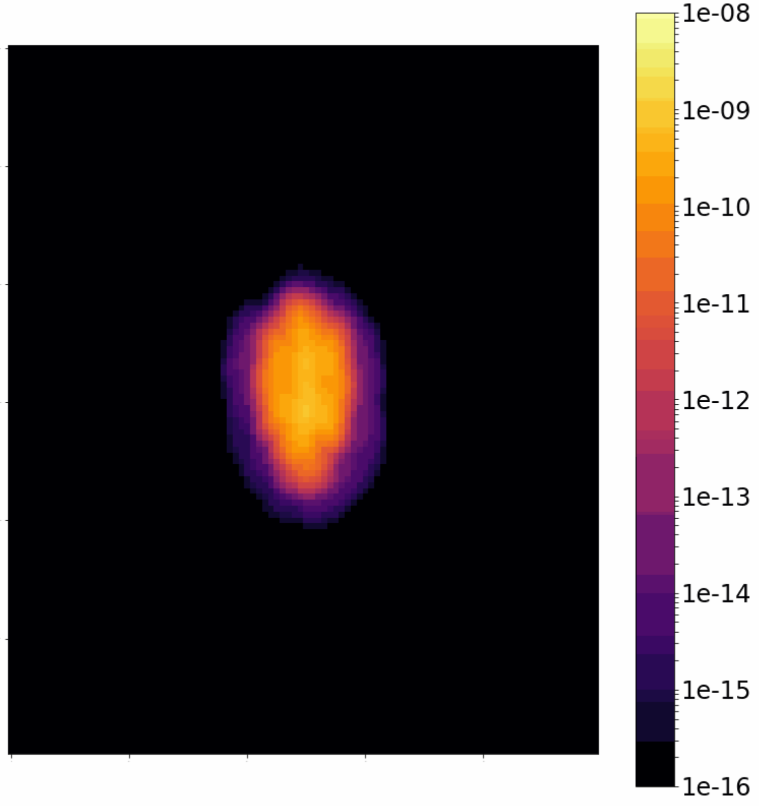

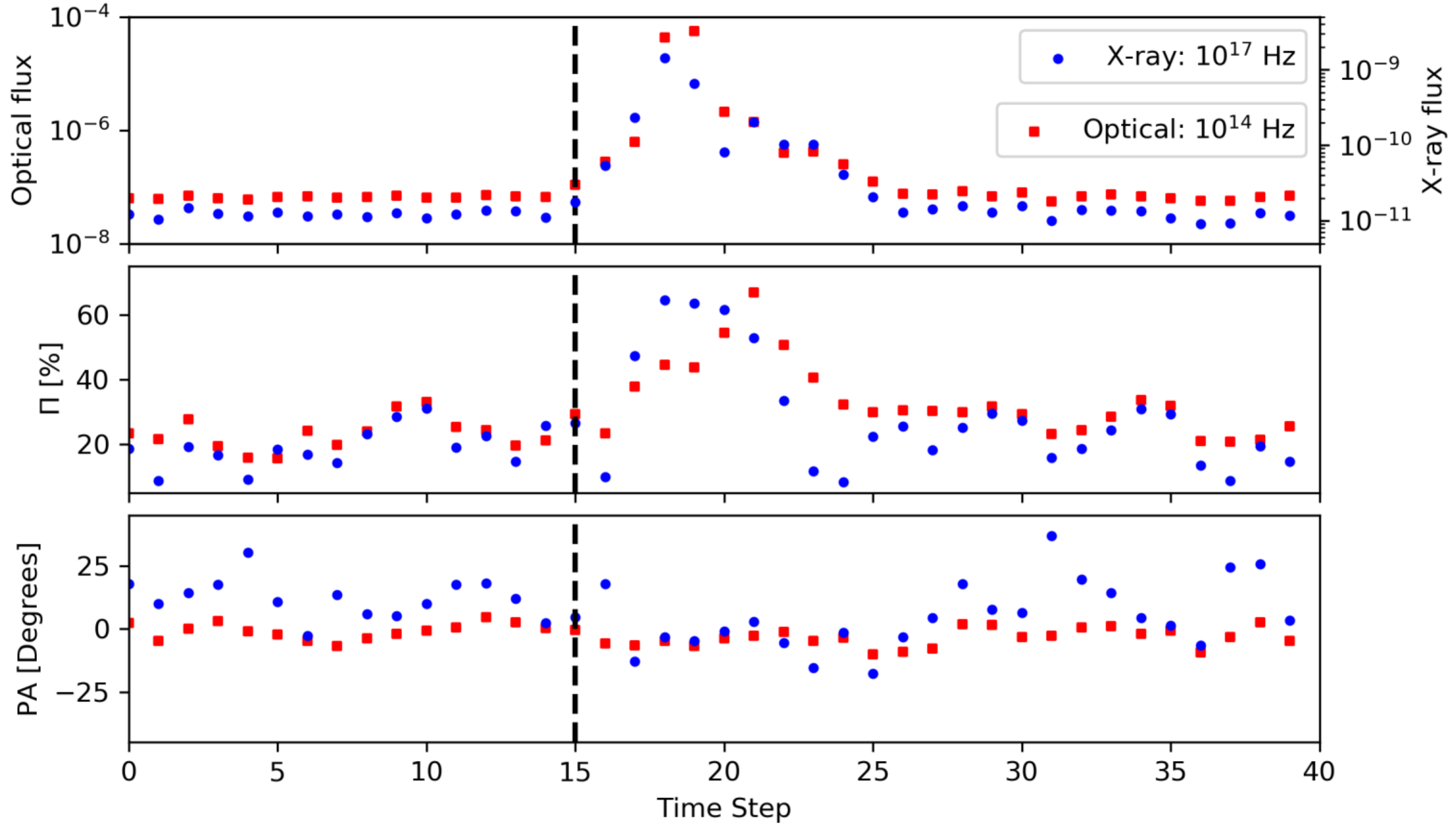

Conclusions

In this study the synchrotron emission of 3D RMHD simulations of the PLUTO code.

- Lagrangian particles were used to represent non-thermal electrons in the jet and used to calculate the synchrotron emission
  - Included synchrotron self absorption
  - Included relativistic effects and light travel time for any viewing angles
  - I,Q, U Polarization calculations
  - Reproduce SED’s

- Reproduced some morphologies and characteristics seen in observations
  - Most simulations showed FR II morphology
    - Radio lobes with hotspots and filaments
  - Reproduced FRI type morphology by inducing deceleration in the jet after injection
  - Bright stationary emission components that correspond to recollimation shocks
  - Filaments and hotspots in lobes correspond to magnetic field structure in cocoon correspond to magnetic

- Variability was investigated in the form of a dense region injected into the jet.
  - Increased in flux coincided with component propagating through recollimation shock
  - X-ray increase lag behind optical
  - Increased flux coincided with an increase in polarization, peak polarization lags behind flux in optical

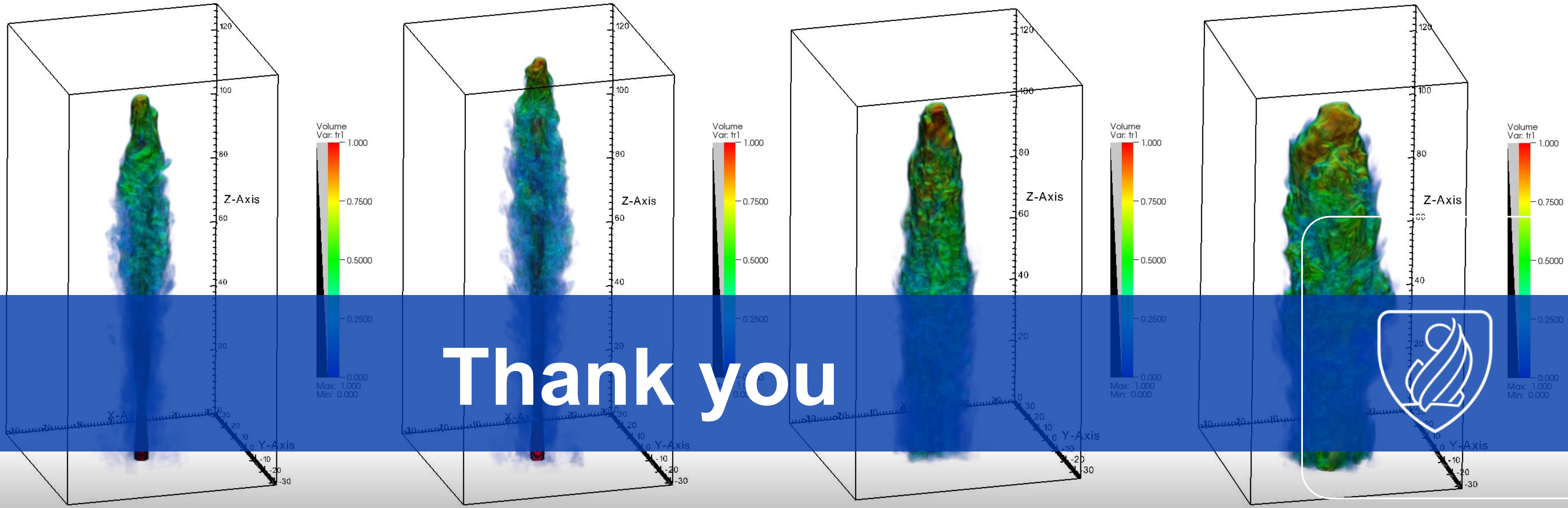

Thank you

www.ufs.ac.za

Inspiring excellence, transforming lives through quality, impact, and care.

VISION130
Renew and Reimagine for 2034

UNIVERSITY OF THE **FREE STATE**
UNIVERSITEIT VAN DIE **VRYSTAAT**
YUNIVESITHI YA **FREISTATA**

UFS
NATURAL AND AGRICULTURAL SCIENCES